HIGH RESOLUTION GEOPHYSICAL IMAGING REVEALS MAJOR FAULTS IN THE SOUTHERN OKLAHOMA AULACOGEN: IMPLICATIONS FOR MID-CONTINENT SEISMIC HAZARDS

By

BRANDON CHASE

Bachelors of Arts w/ Honors in Geology

University of Colorado-Boulder

Boulder, Colorado, USA

2016

Submitted to the Faculty of the

Graduate College of

Oklahoma State University

in partial fulfillment of

the requirements for the Degree of

MASTERS OF SCIENCE

July, 2019

HIGH RESOLUTION GEOPHYSICAL IMAGING
REVEALS MAJOR FAULTS IN THE SOUTHERN OKLAHOMA AULACOGEN:
IMPLICATIONS FOR MID-CONTINENT SEISMIC HAZARDS

Thesis Approved:

_____

Estella Atekwana - Thesis Adviser

_____

Mohamed Abdelsalam

_____

Rob Evans

ACKNOWLEDGEMENTS

This work would not have been possible without the help of my professor, mentor and adviser Dr. Estella Atekwana formerly of Oklahoma State University (OSU) and now at the University of Delaware. Thank you for the many hours of meetings and guidance that all helped to make me a better researcher. I would also like to thank Dr. Mohamed Abdelsalam of OSU and Dr. Rob Evans of Woods Hole Oceanographic Institute (WHOI) for their roles advising my research and offering advice on improving my project.

Thanks is given to the Geological Society of America Graduate Research Grants for partial funding of this work, the Boone Picken's School of Geology Student Enrichment fund for funding conference travel, and the University of Delaware for supporting this project. I would also like to thank WHOI for allowing me to use their facilities, instrumentation, and modeling software in support of this work. Additional thanks is given to Micah Mayle, Steven Johnson, Curtis Carter, David Beckendorf, and John Hager for helping me collect field data. Thank you to the United States Geological Survey and researchers Dr. Carol Finn and Dr. Anjana Shah for making the magnetic data available to me. Finally thank you to Dr. Brett Carpenter, the University of Oklahoma, Molly Simpson-Turko, Chesapeake Energy Corporation, and Seismic Exchange Inc. for providing data, facility use, and support for this research. Special thanks to Folarin Kolawole of the University of Oklahoma for his role in aiding this research, being willing to spend far too long debating ideas on the phone, and for his continued advice on this work.

Special thanks is directed towards Oklahoma State University and the Boone Pickens School of Geology (BPSOG) for providing me with this education. I am grateful for the Tectonics and Structure Research Group for providing me a strong scientific community to work on ideas with. Thanks to all of my friends at OSU who made the school a welcoming and academically productive environment.

To my parents I offer the utmost appreciation. Thank you for your hard work and sacrifice, which has afforded me the opportunity to pursue my education. I would not have been able to get where I am today without your guidance, support and encouragement.

Acknowledgements reflect the views of the author and are not endorsed by committee members or Oklahoma State University.

Name: Brandon Chase

Date of Degree: July, 2019

Title of Study: HIGH RESOLUTION GEOPHYSICAL IMAGING REVEALS MAJOR FAULTS IN THE SOUTHERN OKLAHOMA AULACOGEN: IMPLICATIONS FOR MID-CONTINENT SEISMIC HAZARDS

Major: GEOLOGY

Key Points:

- The fault network in the SOA is composed of NW and E-W trending sets.
- Each set has a major fault related hazard, which are the Meers fault (NW set) and the Willow fault (E-W set). Mohr-Coulomb modelling shows the NW set is at failure in the modern stress field, and the E-W set is well oriented, but not at failure.
- The results suggest the SOA represents a broad regional seismic hazard, which might have several faults capable of producing seismic events of considerable magnitude.

Abstract: While intraplate seismicity can occur anywhere, events frequently localize along preexisting buried basement faults associated with ancient tectonic features and boundaries (ATFBs). Detailed study of these structures can help to determine critically oriented faults vital for intraplate seismic source models and hazard assessments. Here, we use recently acquired high resolution aeromagnetic data over the Southern Oklahoma Aulacogen (SOA), a failed Cambrian rift which experienced inversion during the Ancestral Rocky Mountain orogeny, to provide an unprecedented view of the basement. We integrate the aeromagnetic data with seismic reflection, well-log, remote sensing, field, and earthquake data to assess the modern seismic hazard of SOA faults. Our results reveal the dominance of NW and E-W trending fault sets, the latter of which contains a previously unmapped ~100 km-long E-W trending sinistral strike-slip fault, which we call the Willow Fault. Our results also augment the subsurface extent of the NW trending Meers Fault, the only known seismogenic fault with Quaternary expression in south-central United States. Further, we demonstrate the seismic hazard of the major faults in the SOA; and show that in the current stress field the NW trending Meers Fault is critically oriented, while the additional NW trending faults could represent additional hazards. We also find that the Willow Fault, and the other sub-vertical E-W faults, while not critically oriented in the regional stress field, are not mis-oriented for failure. Recent observations of pronounced natural seismicity along E-W and NW-striking planes in the SOA and the flanking Texas Panhandle underscore the contemporary seismic hazards of the buried structures. The investigative approach and results presented in this study.

TABLE OF CONTENTS

LIST OF TABLES

LIST OF FIGURES

Figure Page

CHAPTER I

INTRODUCTION TO THE SOUTHERN OKALHOMA AULACOGEN

Note:

This thesis is set up to be the manuscript option. Chapter 1 provides a comprehensive overview of the Southern Oklahoma Aulacogen (SOA). Chapter 2 is the manuscript itself. Chapter 3 details future work split between ongoing projects, and possible avenues of research for other workers.

1. INTRODUCTION:

The Southern Oklahoma Aulacogen (SOA) is a NW trending aulacogen in Oklahoma and Texas, where it divides locally into the Wichita Uplift (WU) and Amarillo Uplift (AU), respectively (Fig. 1). The SOA originated as a Cambrian failed rift associated with Rodinia disassembly, and experienced structural inversion in the Late Paleozoic as part of the Ancestral Rocky Mountain (ARM) uplift (Keller and Stephenson, 2007; Leary et al., 2017). Post inversion the SOA has remained tectonically inactive and erosion has resulted in extensive deposition along the northern flank of the SOA, resulting in the hydrocarbon rich Anadarko basin (Perry, 1989)

In the modern day the SOA is a notable seismic hazard in the south central United States (Peterson et al., 2014; Boyd et al., 2015) with seismicity frequently clustering along its length

(Fig. 2). The SOA also houses the Meers fault, which is the only known Quaternary fault in the south central US (Crone and Luza, 1990; Hornsby, 2017). Despite these hazards the SOA still represents a seismic hazard with a poorly constrained internal structure. Here I use this study to map the structure of the SOA, in order to better understand the fault system and map potentially hazardous faults, which are critical for seismic source models (CEUS-SSCN, 2012) and seismic hazard assessments (Peterson et al., 2014).

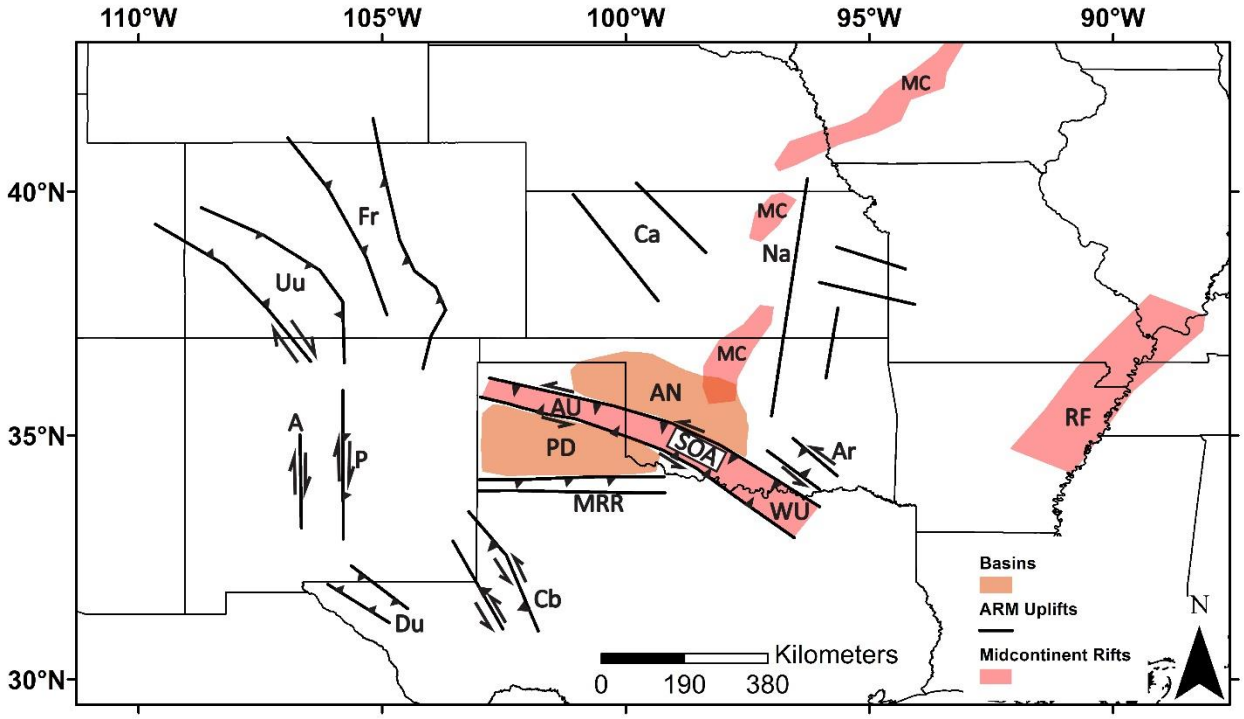

Figure 1: Map showing Ancestral Rocky Mountain related uplifts and midcontinent aulacogens, highlighting the Southern Oklahoma Aulacogen (SOA) as the only feature belonging to both of these subgroups. Modified from Leary et al. (2017) and references therein; relies on Budnik, (1986) and Stein et al. (2014). WU-Wichita Uplift; AU-Amarillo Uplift; Du-Diablo Uplift; Cb-Central Basin Platform; MRR-Matador-Red River Uplift; Ar-Arbuckle Uplift; Na-Nemaha Uplift; Ca-Cambridge Arch; Fr-Front Range Uplift; Uu-Uncompahgre Uplift; P-Perdernal Uplift; A-Albuquerque fault; RF-Reelfoot Rift; MC-Midcontinent Rift; AN-Anadarko Basin; PD-Palo Duro Basin.

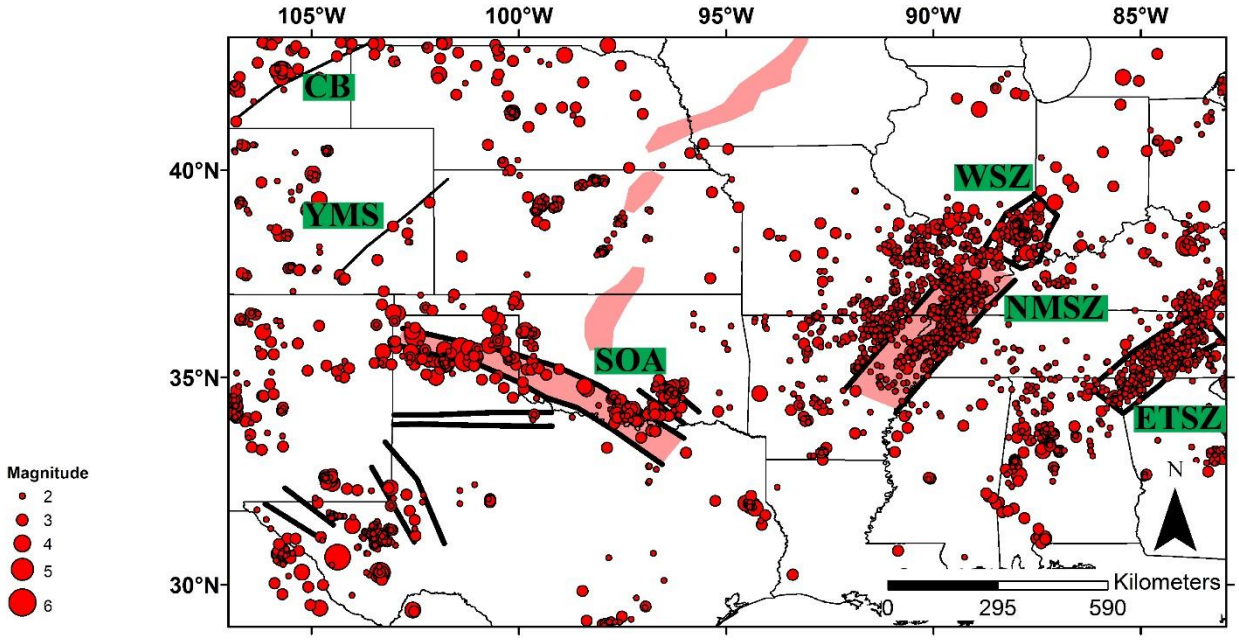

Figure 2: Seismicity in the US midcontinent from USGS catalogs spanning 1900-2019 and from Walter et al. (2018) draped over major tectonic features in the region. Red bodies show paleo-rifts, black lines show borders and/or traces of various tectonic features. Clustered seismicity related to wastewater activities in Texas, Oklahoma, Arkansas and Colorado is not included. ETSZ – Eastern Tennessee Seismic Zone ; NMSZ – New Madrid Seismic Zone; WSZ – Wabash Seismic Zone; SOA – Southern Oklahoma Aulacogen; YMS – Yavapai-Mazatzal Suture; CB - Cheyenne Belt

2.0 GEOLOGIC HISTORY AND SETTING

The SOA originated as the failed rift arm of a rift-rift-rift triple junction during Rodinia disassembly (Hoffman et al., 1974) along a relatively stable southern margin of Laurentia. Rifting is suggested to have initiated in response to a plume impact somewhere around modern Dallas, TX (Hoffman et al., 1974; Burke and Dewey, 1973). The signature of this plume and related rift volcanism is still preserved as anomalously high gravity extending in 3 directions from Dallas: south into Texas, northwest as the SOA, and northeast into Arkansas where it is partially obscured by the later Ouachita orogenic event (Keller and Baldridge, 1995; Keller and Stephenson, 2007). Further support for the plume model comes from modern geochemical sampling of SOA igneous rock, which suggests plume origins for SOA volcanics (Wall et al., 2018; 2019). Initial extension produced the intrusive mafic Glen Mountain Layered Complex

(GMLC) and extrusive Navajoe mountain basalts (Gilbert, 1983; Lambert et al., 1988) (Fig. 3A, B). Faulting, half-graben extension, and rotation of the GMLC followed prior to the intrusion of the Roosevelt Gabbro Plutons (RGP) (McConnell and Gilbert, 1990) (Fig. 3C). Continued magmatism resulted in the Meers Quartzite, Carlton Rhyolite, and Wichita Granites; magmatism ended with the intrusion of late diabase dikes that cut all other igneous rocks in the region, but do not cross the regional unconformity into the overlying Upper Cambrian-Paleozoic Reagan Sandstone (McConnell and Gilbert, 1990; Gilbert, 1983; Ham et al., 1964) (Fig. 3D, E). Rift associated volcanism and magmatic activity within the SOA may be broadly defined into two primary phases. The first was an intercalated mafic gabbro phase (Fig. 3B-D), which was later followed by a more felsic eruption phase (Fig. 3E). These two phases also had various pulses of dolerite dikes emplacement (Gilbert and Hogan, 1998; Hanson et al., 2013). Magmatism is suggested to have occurred from ~539-528 Mya, with the majority of magmatism occurring in an approximately 2 My timeframe from 532-530 Mya (Hogan and Gilbert, 1998; Wall et al., 2018; 2019). On the basis of the extensive magmatism Hanson et al. (2013) has argued that rifting in the SOA was voluminous enough to be classed as a Large Igneous Province (LIP), the only one along the southern margin of Laurentia.

Following the period of extension was a period of rift subsidence and pulses of broad crustal flexure (Amsden, 1982) from the Ordovician to the Devonian. Here marine transgression deposited some 4-5 km of carbonate muds, shelf carbonates, clean sands, and an increasing record of unconformities (Hanson et al., 2013; Gilbert, 1983; Ham et al., 1964) (Fig. 3F, G). Uplift and inversion followed in the Late Paleozoic as part of the wider ARM, a suite of contemporaneous uplifts and deformation features spanning from Chihuahua, Mexico into British Columbia, Canada (Shumaker et al., 1992; Dickerson, 2003; Leary et al., 2017).

Causative forces for ARM uplift remains enigmatic and a variety of tectonic models, frequently competing, exist to explain uplift (e.g. Leary et al., 2017; Marshak et al., 2000; Kluth et al., 1998; Ye et al., 1996; Budnik, 1986; Kluth, 1986; Kluth and Coney, 1981, among a variety of others). Faulting styles also remain controversial with high angle reverse faults being invoked frequently (Leary et al., 2017 and references therein), which are suggested to be reactivated remnants of Precambrian rifting in the region (Marshak et al., 2003).

In the SOA thrust faulting appears to be the dominant method of ARM related uplift (Brewer et al., 1983; McConnell, 1989; Perry, 1989) (Fig. 3B in Chapter II) in line with other south central ARM uplifts (King, 1965; Ye et al., 1996). During inversion approximately 15 +/- 5 km of crustal shortening occurred, along with 12-15 km of vertical uplift (Brewer et al., 1983; Perry, 1989; Keller and Stephenson, 2007). Strike slip movement is also present, but is a point of debate with estimates ranging from a few km to >150 km, and frequently showing the opposite direction of motion (e.g. Leary et al., 2017; Marshak et al., 2003; McConnell, 1989; Granath, 1989; Budnik, 1986 among a variety of others).

Of note in the literature is the argument by Thomas (1991, 2011) who suggests that the SOA, and associated magmatism is due to it being a leaky transform, and not a failed rift. While strike slip movement in the SOA is noted (see above) the large spatial extent of volcanic material noted by Ham et al. (1964), alongside the large volume of at-depth mafic materials (Hanson et al., 2013; Brueseke et al., 2016) is in contrast to the relatively small volume of magmatic material associated with leaky transform systems (Skulski et al., 1991; 1992). Additionally, the geochemical characteristics of SOA magmatic material exhibits tholeiitic, intraplate continental rift affinity, and matches well with known geochemical signature of ocean island basalts and plumes (Gilbert, 1983; Hanson, et a., 2013; Brueseke et al., 2016; Wall et al., 2018; 2019). This

is in contact to leaky transforms, which are usually characterized by alkaline and transitional magmatic affinities (Skulski et al., 1991; 1992). It should be noted that some igneous rocks in the SOA do have alkaline signatures, but these are typically interpreted to represent materials created by either crustal fractionalization or crustal contamination/assimilation (Gilbert, 1983; Hanson, et al., 2013; Brueseke et al., 2016). Finally, Hanson et al. (2013) notes that leaky transforms and rifting are not mutually exclusive, and that strike slip movement attributed to leaky transforms is a common feature of developing rifts. Given the results of these previous works, we will refer to the SOA within the context of a failed rift, when necessary.

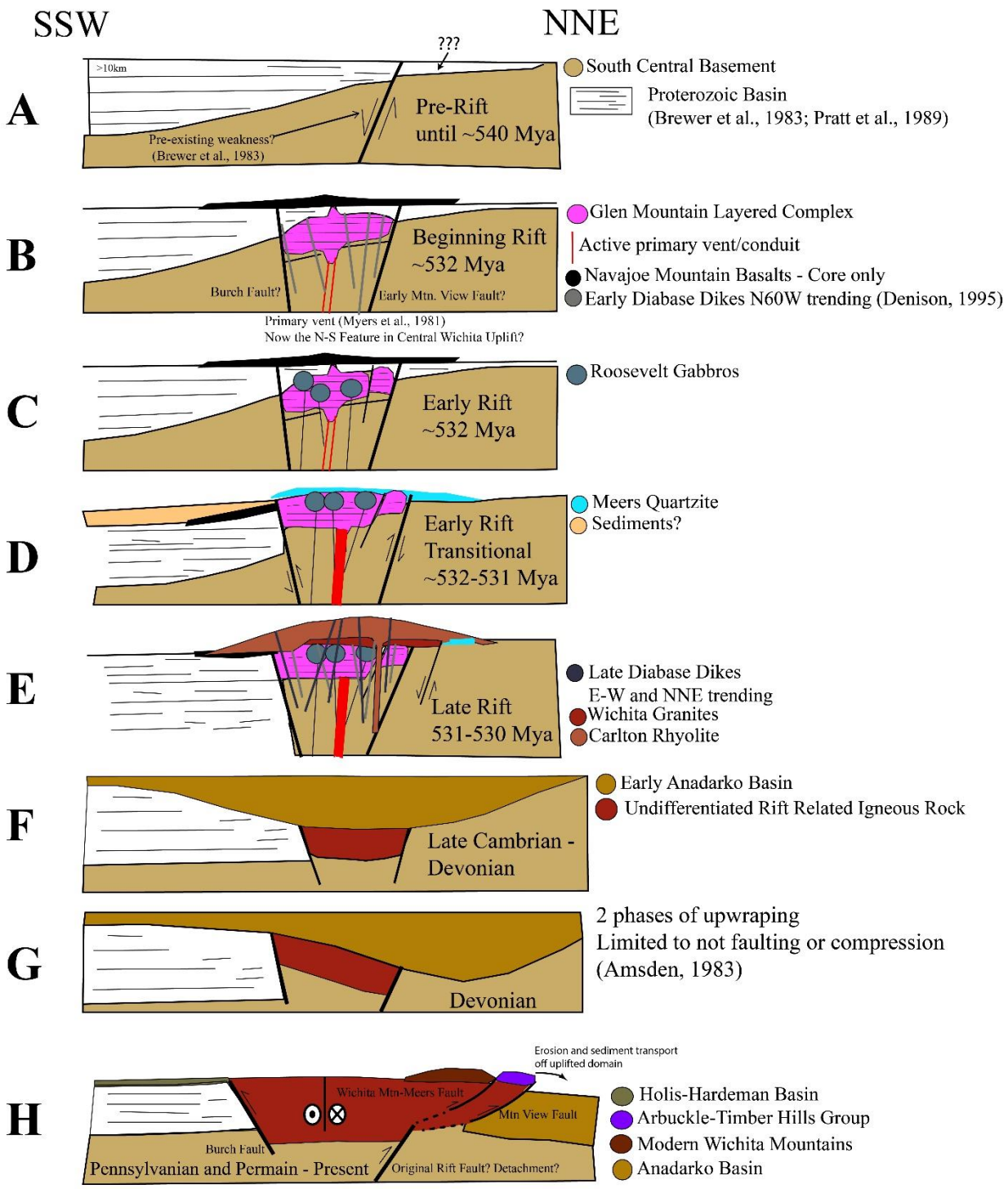

Figure 3. Tectonic history of the SOA. A-E is the rifting phase; F-G is the post rift subsidence phase; H is the post ARM inversion phase. Figure adapted from Gilbert (1983). Relies on Amsden (1982), Brewer et al. (1981, 1983), Donovan (1982), Myers et al. (1981), Keller and Stephenson (2007), Cullen, (2016), Powell et al., (1980), Ham et al. (1964), McConnell and Gilbert (1990); Denison (1995); Wall et al., (2018; 2019); Hanson et al., (2013); Gilbert and Hogan (1998) and this report.

CHPATER II

HIGH RESOLUTION GEOPHYSICAL IMAGING REVEALS MAJOR FAULTS IN THE SOUTH OKLAHOMA AULACOGEN: IMPLICATIONS FOR MID-CONTINENT SEISMIC HAZARDS

B.F. Chase[1], E.A Atekwana[2], M. Abdelsalam[1], F. Kolawole[3], M. Simpson-Turko[3], B.M. Carpenter[3], Finn. C[4]

[1]Boone Pickens School of Geology Oklahoma State University, Stillwater, Oklahoma 74075, USA

[2]College of Earth, Ocean and Environment, University of Delaware, Newark, Delaware 19716, USA

[3]School of Geology and Geophysics, University of Oklahoma, Norman, Oklahoma 73019, USA

[4]United States Geologic Survey Crustal Geophysics and Geochemistry Science Center, Lakewood, Colorado 80255, USA

Corresponding author: Brandon Chase (Brandon.chase@okstate.edu)

ABSTRACT

While intraplate seismicity can occur anywhere, events frequently localize along preexisting buried basement faults associated with ancient tectonic features and boundaries (ATFBs). Detailed structural study of these structures can help to determine critically oriented faults vital for intraplate seismic source models and hazard assessments. Here, we use recently acquired high resolution aeromagnetic data over the Southern Oklahoma Aulacogen (SOA), a failed Cambrian rift which experienced inversion during the Ancestral Rocky Mountain orogeny, to provide an unprecedented view of the basement. We integrate the aeromagnetic data with seismic reflection, well-log, remote sensing, field, and earthquake data to assess the modern seismic hazard of SOA faults. Our results reveal the dominance of NW and E-W trending fault sets, the latter of which contains a previously unmapped ~100 km-long E-W trending sinistral strike-slip fault, which we call the Willow Fault. Our results also augment the subsurface extent of the NW trending Meers Fault, the only known seismogenic fault with Quaternary expression in south-central United States. Further, we demonstrate the seismic hazard of the major faults in the SOA; and show that in the current stress field the NW trending Meers Fault is critically oriented, while the additional NW trending faults could represent additional hazards. We also find that the Willow Fault, and the other sub-vertical E-W faults, while not critically oriented in the regional stress field, are not mis-oriented for failure. Recent observations of pronounced natural seismicity along E-W and NW-striking planes in the SOA and the flanking Texas Panhandle underscore the contemporary seismic hazards of the buried structures. The investigative approach and results presented in this study demonstrate both the seismic hazard of intraplate ATFBs and the method of characterizing the relevant buried faults.

1.0 INTRODUCTION

Earthquakes largely cluster along plate boundaries in response to stress from plate motions. However, infrequent large events like the December 1811 and February 1812 Mw >7.0 New Madrid, 2017 Mw 6.5 Moiyabana, Botswana, and 2011 Mw 5.8 Mineral, Virginia earthquakes (Hough et al., 2000; McNamara et al., 2013; Kolawole et al., 2017) demonstrate that damaging events can occur within stable continental interiors, far from areas of intense strain related to active plate boundaries. Locating many of the causative faults of these earthquakes has historically been after the fact (e.g., McNamara et al., 2013; Kolawole et al., 2017) and frequently, the causative faults remain poorly understood despite concentrated study of singular events (e.g., CEUS-SSCN, 2012). This likely reflects the inherent difficulties of identifying hazardous faults in intraplate regions as tectonic stability, erosion and very long recurrence intervals ranging from 100-100,000 years limit surface exposures and recent surface ruptures (Peterson et al., 2014; Liu and Stein, 2016; Magnami et al., 2017). Thus, of perhaps first order importance is knowing where faults are located, and assessing which represent the most probable hazards in the current stress field, as a way to develop better seismic source models and seismic hazard assessments (CEUS-SSCN, 2012; Peterson et al., 2014), and to help to direct future paleoseismic and geodetic studies.

Since intraplate events tend to cluster near crustal zones of weakness, often associated with ancient tectonic features and boundaries (ATFBs) such as orogenic belts, rifts, failed rifts and sutures (Tuttle et al., 2002; McNamara et al., 2013; Shah et al., 2014; Kolawole et al., 2017; Levandowski et al., 2017), ATFBs represent areas of primary concern and interest. ATFBs are often characterized by litho-structurally distinct fabrics relative to the bounding blocks, thus high

resolution geophysical imaging may be well-suited for delineating the associated buried basement faults to assess their seismic hazards. For example, aeromagnetic data proved useful in revealing the causative faults of the 2017 Mw 6.5 Moiyabana, Botswana earthquake where it was shown the event resulted from extensional reactivation of splay faults within a suture zone (Kolawole et al., 2017).

Recent and historic observations of pronounced natural seismicity along the Southern Oklahoma Aulacogen (SOA) and the flanking Texas Panhandle area (Crone and Luza, 1990; Hornsby, 2017; Walter et al., 2018) presents a major contemporary seismic hazard in south-central U.S. Recently-acquired high-resolution aeromagnetic data over the SOA now affords us the opportunity to investigate the basement structure of the aulacogen and characterize its seismic hazard.

2.0 GEOLOGIC OVERVIEW/HISTORY

The SOA is a NW trending aulacogen located near the Oklahoma – Texas boundary, USA, and is characterized by two major segments: the Wichita Uplift (WU) and the Amarillo Uplift (AU) (inset map in Fig. 1); a minor segment known as the Arbuckle Uplift is also present in south central Oklahoma. The SOA is suggested to be a failed arm of an inferred Rift-Rift-Rift triple junction (Hoffman et al., 1974) that formed during the Late Cambrian break-up of Rodinia (Keller and Stephenson, 2007). Syn-rift magmatism produced intercalated mafic-gabbro and felsic phases, and multiple episodes of diking (Gilbert and Hogan, 1998; Hanson et al., 2013). Post rifting, the SOA was inverted as part of the Pennsylvanian Ancestral Rocky Mountain uplift (Leary et al., 2017). After inversion, the SOA has remained tectonically inactive (Perry, 1989).

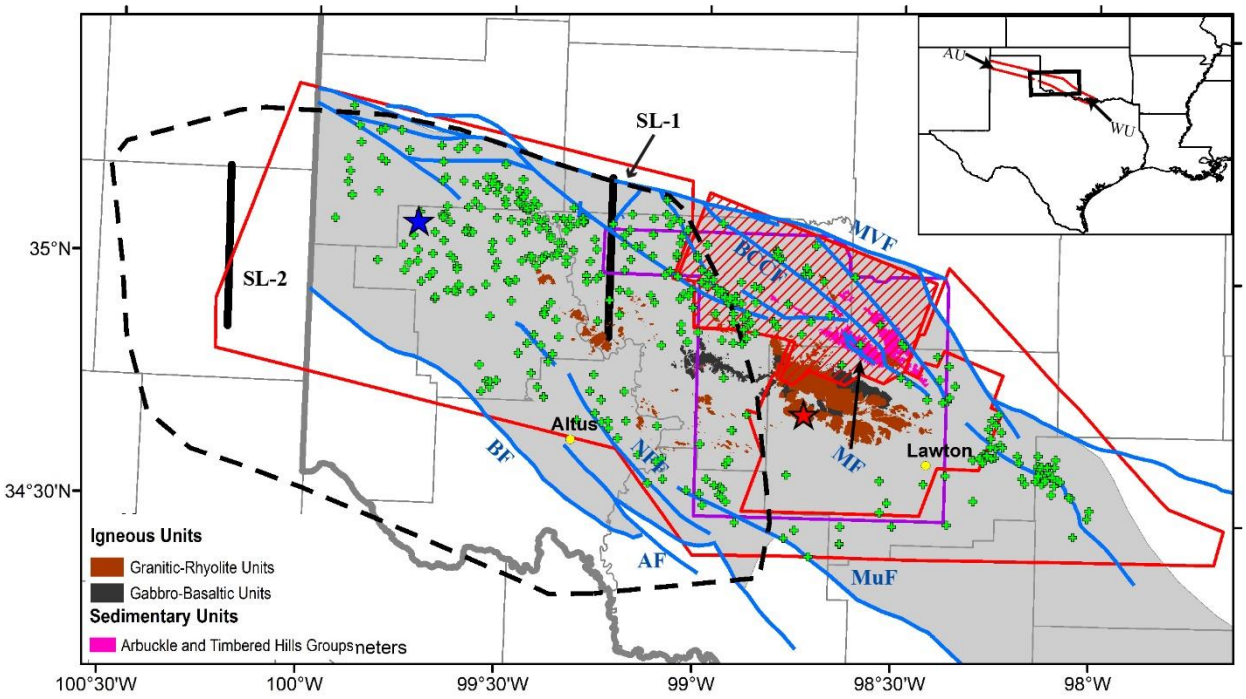

Figure 1: Regional and geologic map of the Wichita Uplift portion of the Southern Oklahoma Aulacogen (SOA) in Oklahoma. The geologic map shows only the exposures of igneous rock associated with the SOA. Red outline indicates the extent of 2017 aeromagnetic coverage; red cross-hatch outline pattern denotes aeromagnetic coverage with 4000m line spacing; purple outline is the 1954 aeromagnetic data; grey shaded region is the historical subsurface extent of the Wichita Uplift section of the SOA in southern Oklahoma; black dotes are cities; vertical black lines denote the seismic lines in Fig. 3B, C; black dashed line is the depth to basement coverage and the green are the wells used (Fig. 3a); colored stars are field locations studied in Fig. S2. Geologic units and the Wichita Uplift subsurface extent are modified from maps produced by the Oklahoma Geological Survey (OGS). Blue lines are major mapped faults from Hollard, 2015 and are MVF-Mountain View Fault; BCCF-Blue Creek Canyon Fault; WM-MF-Wichita Mountain-Meers Fault; NFF- North Fork Fault; BF-Burch Fault; MF-Muenster Fault; AF-Altus Fault. Inset map displays the Amarillo Uplift (AU), Wichita Uplift (WU).

3.0 DATA AND METHODS

3.1 Aeromagnetic Data

We use two high-resolution aeromagnetic datasets acquired in 1954 ('Wichita') and 2017 by the United States Geological Survey ('2017'), and the lower-resolution North American Magnetic Anomaly Map (NAMAM) data to fill the data gaps (high-resolution survey areas are in Fig. 1). Technical details for the survey, links to the data, and relevant sources can be found in Table S1 in the online supplement. These data were knitted together to produce seamless

magnetic maps over the region (Fig. 2). Additional details on knitting, aeromagnetic theory and aeromagnetic filtering can be found in the supplementary section below.

Prior to data knitting, we reduced the residual anomaly grid of each of aeromagnetic datasets to the pole (RTP) (Baranov, 1957; Arkani-Hamed, 1988) in order to position magnetic anomalies directly over their causative sources. After the datasets were then knitted together, we applied upward-continuation the aeromagnetic data to increasing depths to assess the subsurface extents of target structures (Jacobsen, 1987). Finally, we applied vertical derivative filters to resolve the edges related to subsurface structures (Miller and Singh, 1994) (Figs. 2A and Fig. S1).

According to standard practice, edges in the filtered aeromagnetic data can be interpreted as abrupt terminations related to fault offsets, dikes, and changes the trends of basement foliation (e.g., Grauch and Hudson, 2007, 2011; Blakely et al., 2000; Kolawole et al., 2017, 2018). These observations are consistent here, particularly along the well-studied Wichita Frontal Thrust (WFT), between the Mountain View and Wichita Mountain-Meers Fault (Fig. 1), where spatial correspondence is observed between magnetic derived faults and known faults (overlapping blue and black lines in Fig. 2B).

3.2 Other Datasets

We integrate the aeromagnetic data with other available subsurface datasets, generate basement structure map from well logs (Fig. 3A), and interpret shallow subsurface geometry of target faults from 2-D seismic reflection data. Further, we analyze satellite fracture orientations over the exposed Cambrian WU granites (Fig. 2D). Finally, we use field structural data (Fig. 2E;

S2) to ground truth the aeromagnetic, satellite, and seismic data interpretations. Additional details can be found in the supplementary section below.

4.0 RESULTS AND DISCUSSION

4.1 Basement Fault Systems

Our filtered aeromagnetic maps provide details on the basement structure of the WU, which is dominated by a NW trending central region of high amplitude and short wavelength magnetic lineaments/edges surrounded by a region of more subdued magnetic anomalies (Fig. 2A and S1). Faults traced from the aeromagnetic data dominantly trend 280° (±3°) (~E-W) and 330° (±4.5°) (~NW) (Fig. 2C) while fractures and faults in the remotely sensed data trend 272° (±6.2) (~E-W) and 12° (±11.5) (~NNE) (Fig. 2D). To understand the kinematics of the large satellite fractures and faults in WU granites we integrate structural mapping of McLean and Stearns (1986) Fig. 2E) who suggest the E-W set commonly shows sinistral strike-slip offsets, whereas the NNE fractures show predominately dextral strike slip offsets. Interestingly, both trends also parallel field measurements of Cambrian rift-related dike trends (Fig. S5).

The magnetic data highlights the largest structures of these trends as the NW trending Meers Fault, a known seismogenic fault (Crone and Luza, 1990; Hornsby, 2017) and a previously unrecognized 100-110 km E-W trending magnetic low (herein referred to as the Willow Fault after Willow, Oklahoma) (Fig. 2). As the largest single fault of the E-W set much of our focus on this set is directed towards the Willow Fault. The upward continued aeromagnetic maps show the Willow Fault extends to at least 7.5 km depth (Fig. S1A-D), and while we lack unequivocal piercing points we follow Blakely et al. (2000) and use the shift in

anomalies to provide reasonable displacement estimates. This approach suggests ~40 km of maximum sinistral movement on the Willow Fault (yellow bars in Fig. 2A).

In the 2-D seismic reflection profiles and well penetration basement structure map, the Willow Fault shows: (1) minimal vertical offsets, but disrupts seismic reflectors of the overlying Permian strata in the east (Fig. 3A, B); (2) ~460 m of vertical offset in the basement and folding in overlying Permian strata (Fig. 3C) in the west, which corresponds to monocline folding and surface fractures in the west (Fig. S2C, D); and (3) modifications of depth to basement along trace (Fig. 3A). Coupling this last observation with aeromagnetic depth analysis shows the Willow Fault is deeply rooted in the basement. Hence, we interpret the Willow Fault as a basement rooted, steeply dipping, sinistral strike slip fault, with a small component of oblique slip.

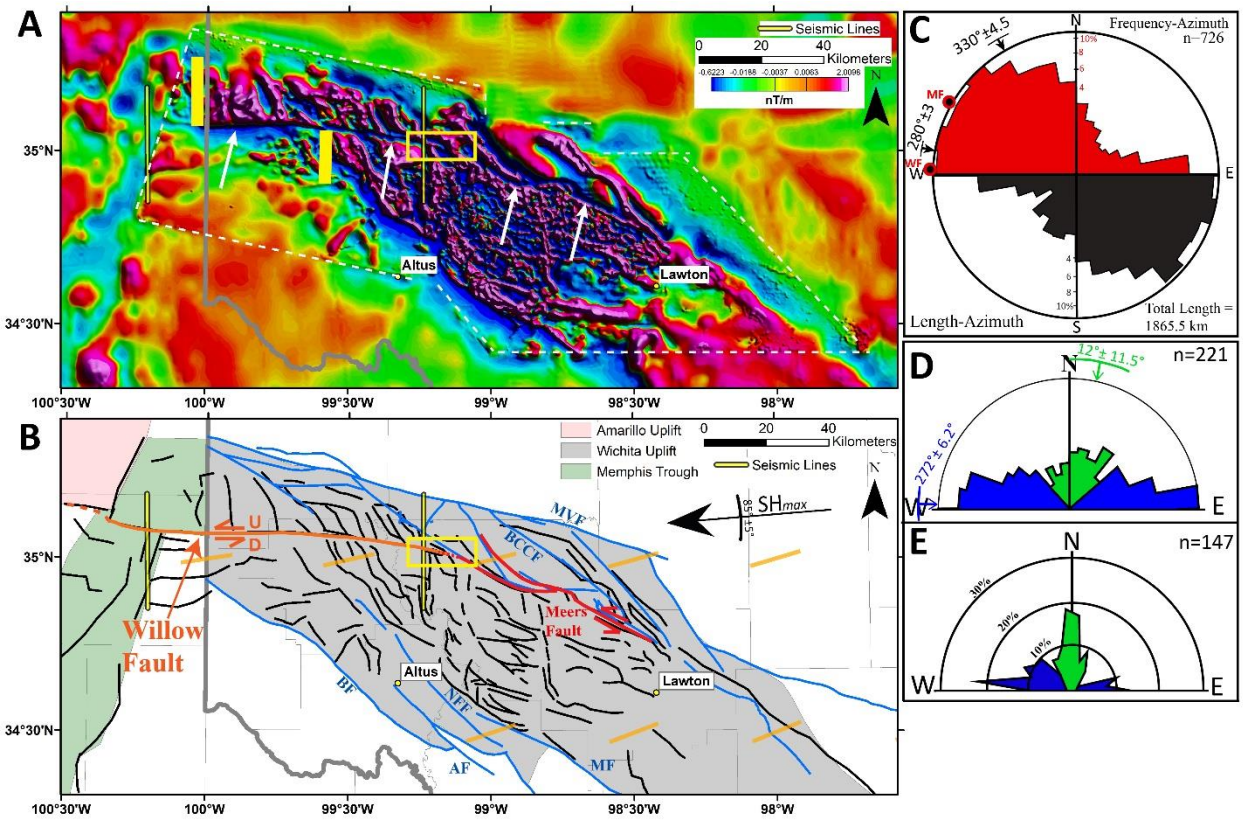

Figure 2: A) Reduced to Pole (RTP) 2017 magnetic data that has been upward continued to 400 meters and had the First Vertical Derivative (FVD) taken. White arrows point to the Willow fault; yellow box is the possible connection zone for the Meers and Willow faults; white dashed lines mark suturing artifacts. B) Structural interpretations map derived from A. Black lines correspond to aeromagnetic lineaments and faults; red line corresponds to the Willow fault, Meers fault, and their connection; shaded regions are tectonic historic or magnetic domains of note; black SHmax orientation is the regional value used for Mohr-Coulomb modeling and is from Alt and Zoback (2016); faded orange bars are SHmax orientations from Heidback et al. (2018); blue lines are the same major faults as Fig. 1. C) Orientation of fault segments derived from the magnetic data with the Willow Fault (WF) and Meers Fault (MF) orientation overlaid. D) Rose diagram of fractures and faults mapped in exposed granites in the Wichita Uplift from 60 km eye altitude satellite data. E) Fracture and fault orientations sense of offset modified from McLean and Stearns (1986); green indicates right lateral; blue indicates right lateral. Color scheme is the same as in D. Note the similar trends.

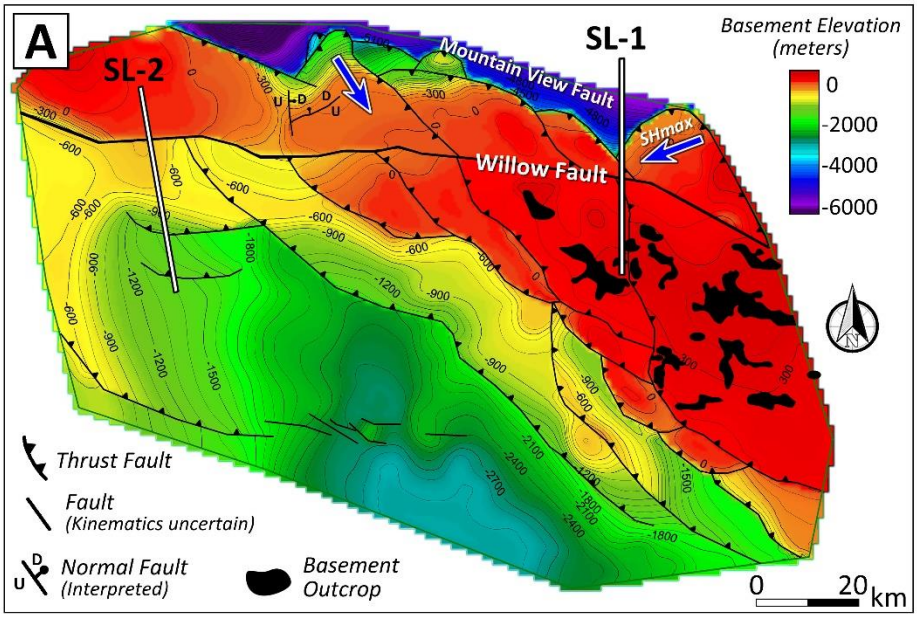
A
SL-2
SL-1
Mountain View Fault
Willow Fault
SHmax
Basement Elevation
(meters)
0
-2000
-4000
-6000
Thrust Fault
Fault
(Kinematics uncertain)
Normal Fault
(Interpreted)
Basement
Outcrop
0
20 km

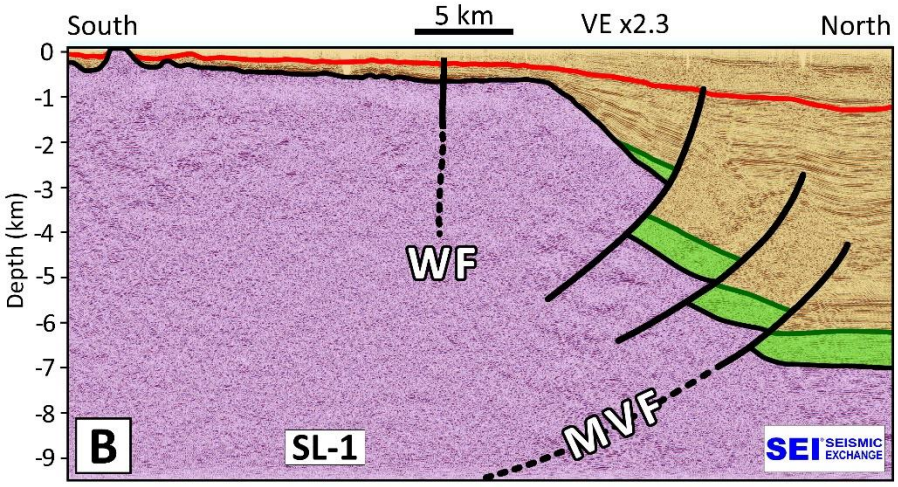
South
5 km
VE x2.3
North
Depth (km)
WF
MVF
B
SL-1
SEI SEISMIC EXCHANGE

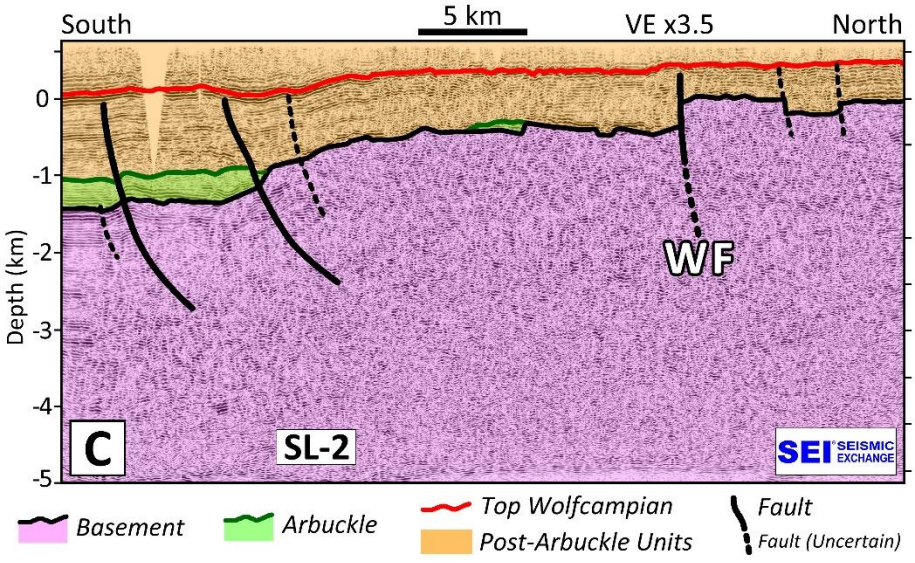
South
5 km
VE x3.5
North
Depth (km)
WF
C
SL-2
SEI SEISMIC EXCHANGE
Basement
Arbuckle
Top Wolfcampian
Post-Arbuckle Units
Fault
Fault (Uncertain)

Figure 3: A) Depth to basement coverage from well data, see figure 1 for location and well coverage. B) Eastern seismic line showing limited vertical displacement along the Willow fault (WF) but disruptions in overlying sedimentary packages. C) Western seismic line showing more vertical displacement along the WF and monocline folding in the overlying sedimentary packages. Refer to Fig. S3 for interpreted seismic sections.

4.2 Seismic Hazards

The igneous basement of Oklahoma exhibits frictionally unstable behavior at the depths of observed earthquakes (Kolawole at al., 2018b), and slip is dominantly strike-slip to normal when faults reactivate in the current ~E-W stress field (e.g., Alt & Zoback, 2017). Occurrences of recent natural seismicity within the WU, AU and flanking regions (Gordon, 1988; Walter at al., 2018; Fig. 4B), and the geomorphic expression and Holocene paleoseismicity of the Meers Fault system (Crone and Luza, 1990; Hornsby, 2017) indicate the presence of seismic hazards associated with basement rooted faults along the SOA (e.g. Boyd et al, 2015). The bulk of these faults can be grouped into either a ~E-W or ~NW set, with the major faults for each being the Willow and Meers Faults, respectively. A smaller ~N-S set is also present but does not appear to constitute many major structures (Fig. 2C).

To better understand the hazard of the two major faults and similar trending faults, we consider the Mohr-Coulomb criterion for fault reactivation. Previous studies of Oklahoma basement faults and seismicity provide constrains on mechanical parameters of the faults (Table S1). Mean stress field (SHmax) orientation and magnitude at ~5km basement depth (Alt and Zoback, 2017), cohesion and coefficient of static friction of intact and pre-existing fault basement rock (Katz et al., 2001; Kolawole et al., 2018b) and geometries of target faults from geophysical data (this study) are used to assess nearness of failure for each fault set.

Our analysis (Fig. S3) suggests that in the current strike-slip to reverse-strike slip stress state along the WU (Lund-Snee and Zoback, 2016) the ~55 km-long Meers fault is critically

oriented for failure. These observations underscore the current seismic hazard of the Meers Fault system and build on the hazard determined by paleoseismic work over the Meers, which has suggested that 3-4 Holocene events have occurred along the fault, with the strongest being a Ms ~7.0 (Crone and Luza, 1990; Hornsby, 2017). These observations argue also argue that the ~100 km-long Willow Fault, which has similar geometry, occurs in similar basement lithologies, and hosts similar surface monocline warping (Fig. S2D; Hornsby, 2017) could also be capable of a Meers Fault-like seismic rupture. We do note that while our Mohr-Coulomb analysis shows the Willow is not currently critically oriented for failure it is however not-misoriented for failure. Further, while we opted for a more regional SHmax orientation for use in our Mohr-Coulomb modelling we note that Heidback et al. (2018) and the World Stress Map Project suggested SHmax rotates closer to ~NE near the WU (Fig. 2B, 4B). This possible stress rotation would result in the Willow Fault being more critically oriented for failure.

In the western SOA stress field data in the AU is limited to only a few points but appears to be similar to that observed regionally in Oklahoma (Heidback et al. 2018). The few known faults in the AU (Ewing et al., 1990) and those interpreted from the low resolution aeromagnetic data show similar orientations to WU faults (Fig. 4B), suggesting a population of faults with similar orientations. Given both uplifts are a part of the SOA and are genetically related AU faults likely behave similar to WU faults. Walter et al. (2018) recently cataloged a variety of natural events in the AU missed in other catalogs, and we note many spatially correspond to Meers and Willow like oriented faults, while the few focal mechanisms also suggest activity along fault planes trending subparallel to W and NW (Fig. 4B). While there is a clear need for collection of subsurface data and increased seismic monitoring of the SOA the reliance on small earthquakes to predict large ones (CEUS-SSCN, 2012), paired with the spatial localization of

recorded events, focal mechanism data, similar fault orientations and a similar stress field highlights that many of the AU faults constitute hazards similar to the Meers, Willow and similar trending faults.

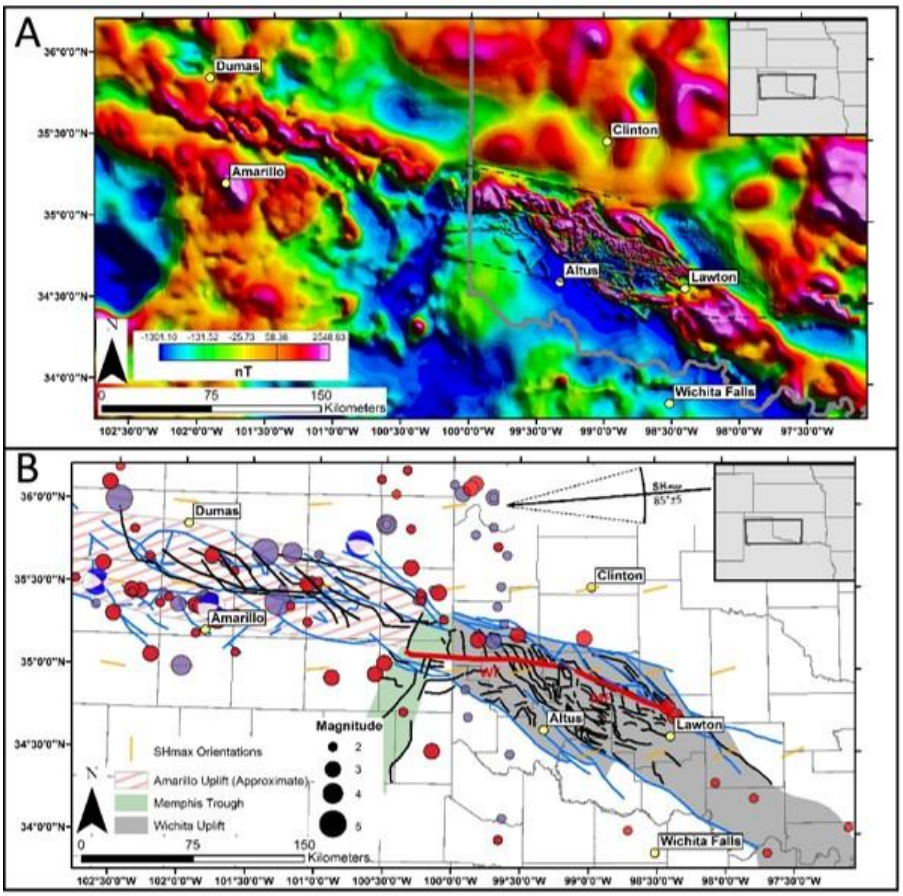
A
Dumas
Clinton
Amarillo
Altus
Lawton
Wichita Falls
nT
Kilometers
B
Dumas
Clinton
Amarillo
Altus
Lawton
Wichita Falls
Magnitude
SHmax Orientations
Amarillo Uplift (Approximate)
Memphis Trough
Wichita Uplift
Kilometers

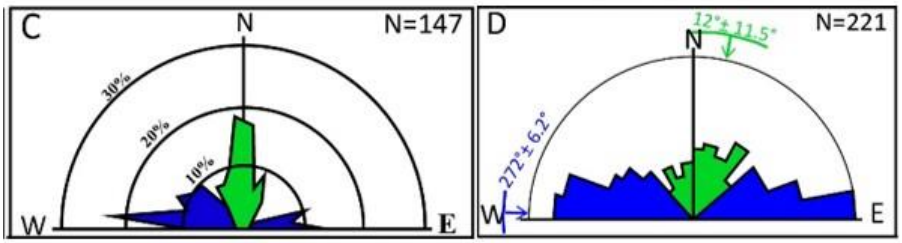
C
N
N=147
30%
20%
10%
W
E
D
N
N=221
12° ± 11.5°
272° ± 6.2°
W
E

F

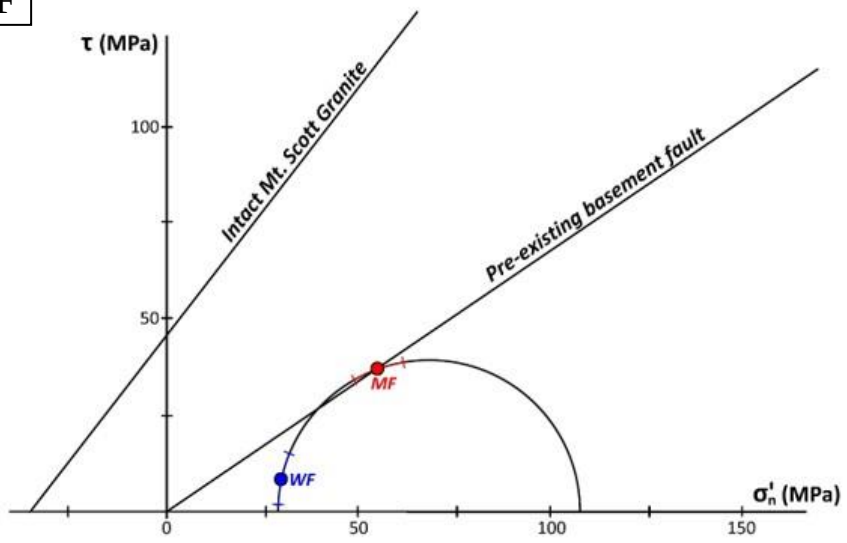
τ (MPa)
100
50
Intact Mt. Scott Granite
Pre-existing basement fault
MF
WF
0
50
100
150
σ'n (MPa)

Figure 4: A) Reduced to Pole (RTP) Regional Total Magnetic Intensity (TMI) map of the Southern Oklahoma Aulacogen (SOA) of the high resolution data and MAMNA data; black dashed lines denote knitting artifacts. B) Interpretations for each SOA terrain based on this data and from Fig. 2B; black lines correspond to structures from Fig. 2B and those interpreted from the lower resolution MAMNA data; orange bars are the same SHmax orientation displayed in Fig. 2; the larger SHmax orientation is the direction used for Mohr-Coulomb modelling from Alt and Zoback (2016); red circles are earthquakes from the USGS catalog from 1900-2019; purple circles are earthquakes from Walter et al. (2018); blue lines are regional faults from Marsh and Holland (2016) and Ewing et al. (1990); focal mechanisms are from Saint Louis University Earthquake Center; earthquake events display natural seismicity, and the bulk of non-natural events in central Oklahoma have been removed. D) Rose diagram of fractures and faults mapped in exposed granites in the Wichita Uplift from 60 km eye altitude satellite data. E) Fracture and fault orientations sense of offset modified from McLean and Stearns (1986); green indicates right lateral; blue indicates right lateral. Color scheme is the same as in D. Note the similar trends. F) Mohr-Coulomb failure modelling for the Meers Fault (MF) and Willow Fault (WF), and their respective fault sets.

5.0 Conclusions

Overall, the SOA is defined as an ATFB composed NW and E-W trending faults, with the NW set, and Meers Fault, being critically oriented in the current stress field and constituting much of the hazard posed by the SOA over a broad region. The E-W set, and Willow Fault, may represent possible additional hazard depending on previously proposed stress field rotations near the SOA by Heidback et al. (2018). While there is a need for increased seismic monitoring of the SOA, this study demonstrates that the SOA may represent an underweighted seismic hazard in the region. This study also demonstrates the value of collecting high resolution aeromagnetic data for its ability to constrain fault systems in hazardous ATFBs, which can be used to directed future geodetic and paleoseismic work. Extending this approach to other ATFBs with deeply buried faults will impose limits on the resolving power of high resolution magnetic surveys, but those faults with the greatest hazard potential and activity likely rupture into overlying sedimentary strata. In these cases an approach similar Grauch and Hudson (2007), which is useful for highlighting sedimentary faults with magnetic data, may be useful in these cases.

6.0 ACKNOWLEDGEMENTS

We thank Anjana Shah for providing the 2017 magnetic data to Oklahoma State University; Seismic Exchange Inc. (SEI) and Chesapeake Energy for access to their seismic data and facilities. Partial support for the project was provided by the Geological Society of America Graduate Student Research Grants program

7.0 SUPPLEMENTARY SECTION

7.1 Main Text Supplementary Figures

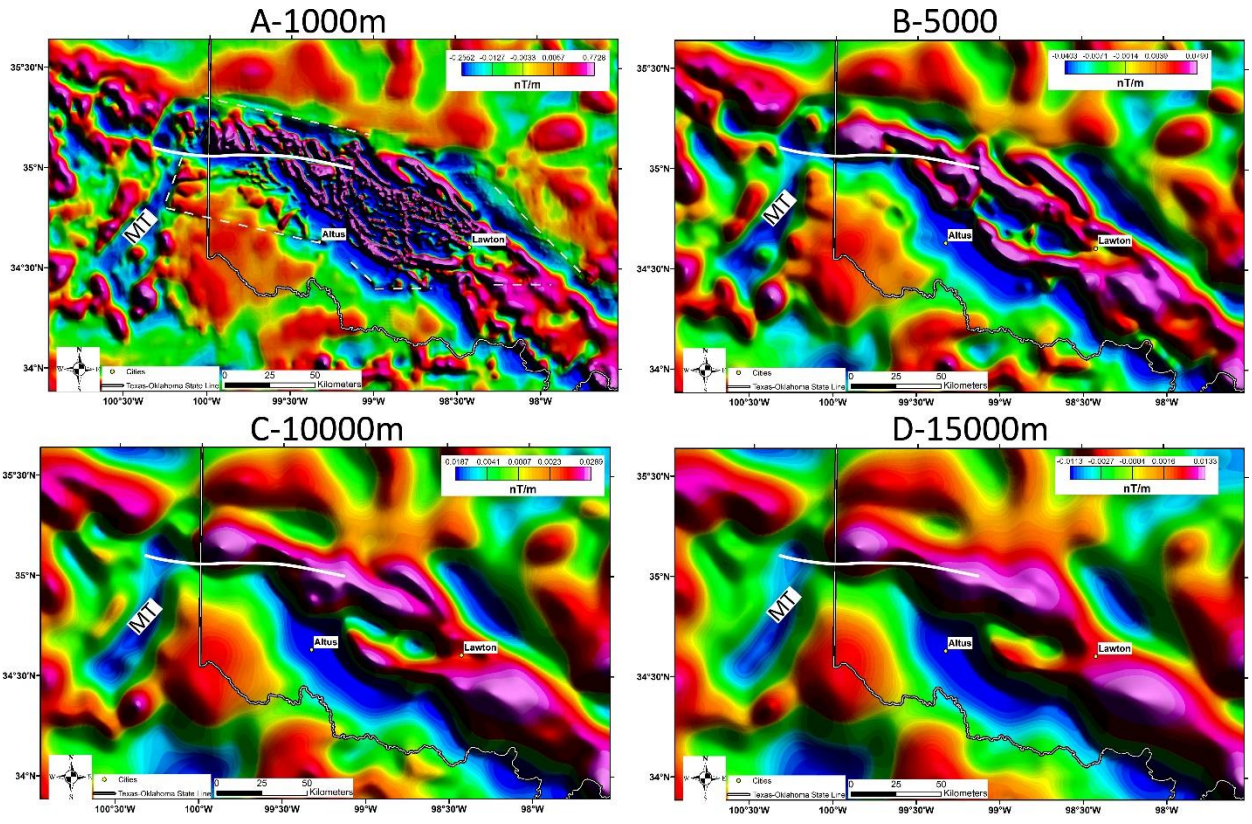

Figure S1. Sutured magnetic data that has been Reduced to Pole (RTP), had the vertical derivative taken, and been upward continued to various elevations to show depth extent of structures in the Wichita Uplift region and along the Willow Fault (see Fig. 2 for comparison). The value by which data has been upward continued by is displayed next to the tiles letter. One-half of the upward continuation elevation added to flight height is the approximate depth (Jacobsen, 1987). Given survey flight elevation was an average of 140 m, and these depths are

approximation, the role of flight height is minimal compared to upward continuation filtering. The white line is the Willow fault trace and MT is the Memphis Trough domain. White dashed lines (only needed in panel A) correspond to suturing artifacts that have been highlighted to avoid possible misinterpretation.

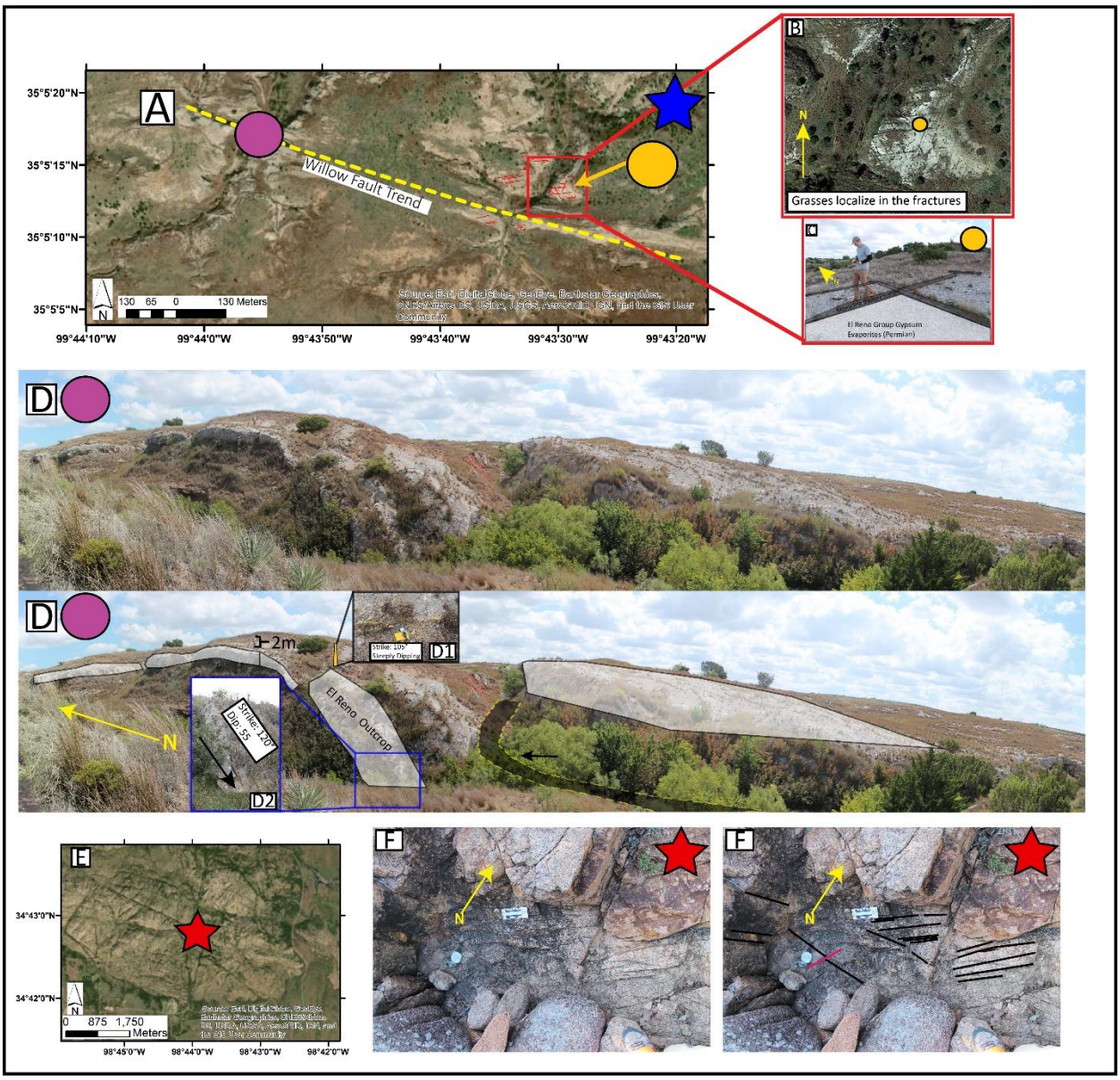

Figure S2. Summary of the in-field structural analysis of a monocline flexure above the Willow Fault. Star symbols are color coded and correspond to the location stars in Fig. 1. A) Locations of study first field site. The circles are color coded and mark the locations of S2B, C, and D. Yellow line is the possible fault trace of possibly the Willow Fault or related splay structure; red lines are fractures. B) Zoomed fractures from A. C) Ground level expression of the fractures localizing grass growth. D) Un-interpreted and interpreted surface monocline folding consistent with observations in the seismic data. E) Location of second field site. F) Un-interpreted image and interpreted images showing fractures observed.

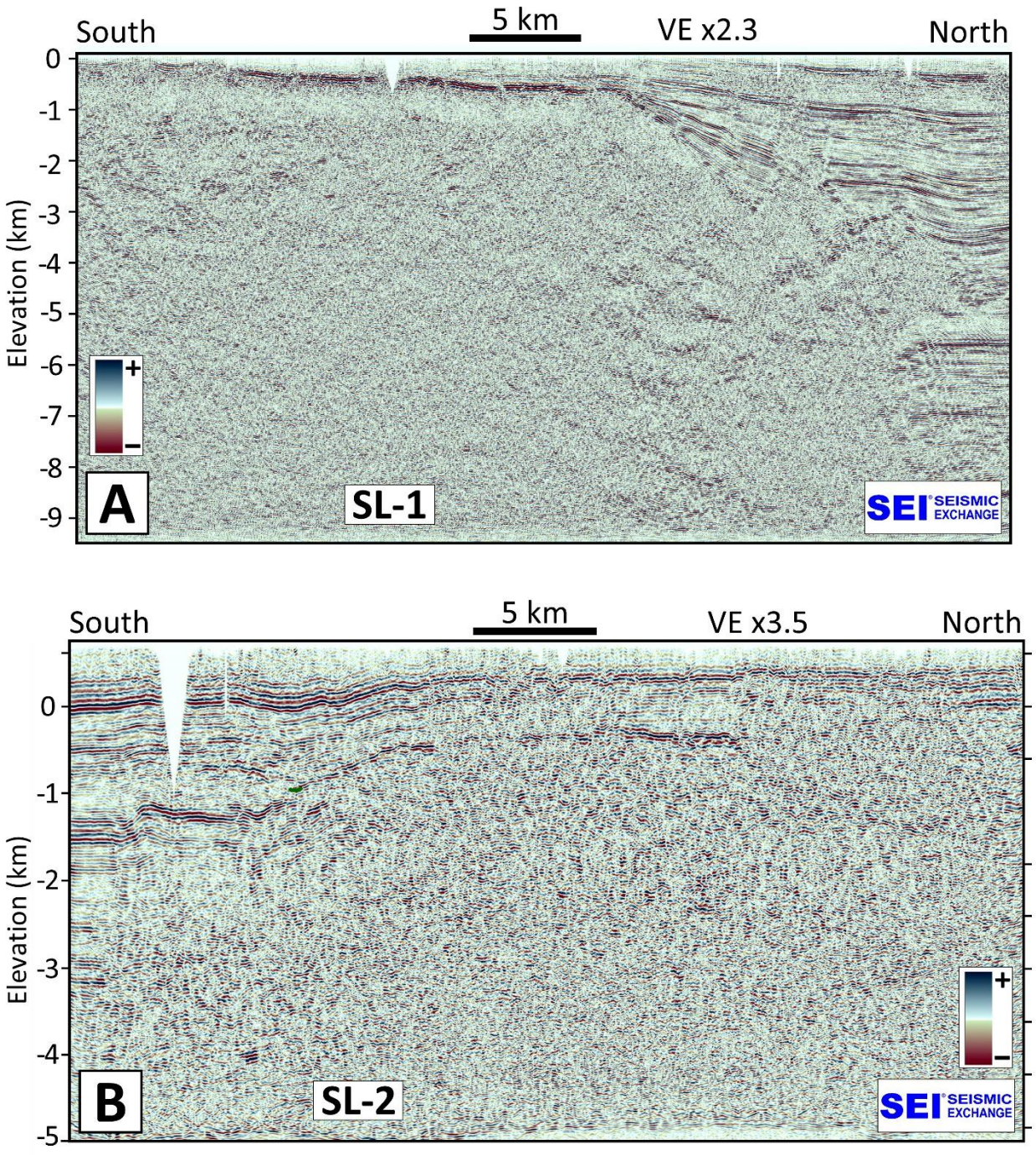

Figure S3. A) Uninterpreted western seismic section SL-1. B) Uninterpreted seismic section Sl-2.

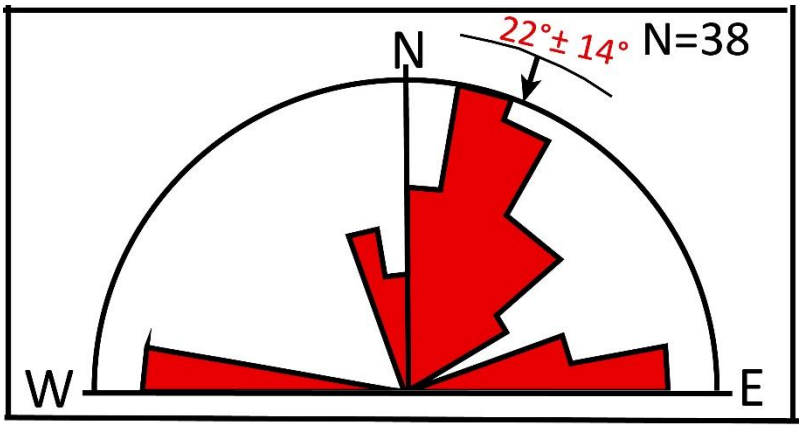

Figure S4. Compilation of dike measurements in the Wichita Uplift using data from this study, Johnson (1955), McLean and Stearns (1986), and Al-Shaieb (1988).

7.2 Supplementary Tables

Survey Year and Name	Data Website	Notes	-Flight height -Line Spacing -Flight direction -Tie line spacing/direction (m)
2017 – "2017"	https://www.sciencebase.gov/catalog/item/5a9f0b3ce4b0b1c392e50241	Data and contractor report containing survey technical details can be found here.	-138 -400 w/ 200m infill -NE-SW -4000/E-W
1954 – "Wichita"	https://pubs.usgs.gov/ds/2005/138/neksok.html Click "Get Data"	Survey data and secondary processing done by Sweeney and Hill (2005) can be found here.	-152 -402 -E-W -unknown
1974 to 1981 – "NURE" Variety of years - "National Magnetic Anomaly Map of North America" or "NAMAM"	https://pubs.usgs.gov/of/2009/1129/NURE.html For Individual State Grids https://mrdata.usgs.gov/magnetic/ https://crustal.usgs.gov/projects/namad/#US For United States national grid and individual surveys	Interested users of this data are advised to read the respective Metadata for the national map, individual surveys, and individual NURE 'blocks.' Resolution changes frequently from area to area and frequently better resolution data than the NAMAM grid displays is available in specific areas. Survey data and technical details can be found for individual surveys or for the entire NAMAM grid.	-121 -~4800 -E-W -single cross continental tie line

Table S1. Details for the aeromagnetic data used in this survey.

Parameter	Mean Value	Notes
Stress State	N/A	Strike-slip state is determined from A_phi in Lund Snee & Zoback (2016)
Coefficient of friction (intact rock)	1.31	Mount Scott Granite (Wichita Uplift, Southern Oklahoma) from Katz et al. (2001)
Cohesion (intact rock)	46 MPa	Mount Scott Granite (Wichita Uplift, Southern Oklahoma) from Katz et al. (2001)
SHmax	155.42 MPa	Mean SHmax magnitude for Oklahoma, from Walsh & Zoback (2016)
SHmin	76.6 MPa	Mean SHmin magnitude for Oklahoma, from Walsh & Zoback (2016)
SHmax orientation	085° ±5	Mean SHmax for Oklahoma, from Alt & Zoback (2016) at 5-6 km depth
Pore pressure	47.5 MPa	Natural pore pressure distribution of 45.2 to 50.9 MPa bounds (Nelson et al., 2015; Walsh & Zoback, 2016). Mean estimate is for 5 km depth.
Coefficient of friction (pre-existing Basement Fault)	0.68	Oklahoma granite basement faults from Kolawole et al., 2018
Meers Fault Geometry:		
Strike	300°	Surface trace and aeromagnetic data (this study)
Dip	89°	From Jones-Cecil (1995); dip of steep Oklahoma basement faults in Walsh and Zoback (2016)
Willow Fault Geometry:		
Strike	91°	Aeromagnetic data and mean trend of surface deformation (this study)
Dip	89°	From Jones-Cecil (1995); dip of steep Oklahoma basement faults in Walsh and Zoback (2016)

Table S2. Parameter values used for the Mohr-Coulomb Failure Analyses of Oklahoma basement faults.

8.0 AEROMAGNETIC DATA USED AND GRID KNITTING

We use two high resolution aeromagnetic datasets acquired in 1954 ('Wichita') and 2017 ('2017') by the United States Geologic Survey, alongside the more coarse North American Magnetic Anomaly Map (MAMNA) data, which is used to fill in data gaps between the two higher resolution surveys (high resolution surveys drawn in Fig. 1 in Chapter 2). Specifications for the Wichita, 2017 and MAMNA datasets, respectively, are as follows. Average flight height (m): 152, 138, 12; Line spacing (m): 402, 400 with 200 infill, and 4828. Flight direction: E-W, NE-SW, E-W. Tie Lines/Direction (m): single cross-continent, 4000 E-W, single tie line flown. These data were knitted together to produce seamless magnetic maps over the region (Figs. 2 and 4 in Chapter 2). The associated magnetic datasets, and further technical information, may be found in the links provided in Table S1.

All magnetic knitting was done in the Oasis Montaj software package using industry standard techniques. All grids are displayed with the default color hill shade. Below are the processing steps used for grid-knitting:

First, subsets (known as 'masks') of the MAMNA map, which is largely National Uranium Resource Evaluation (NURE) data in Oklahoma and Texas, were taken to examine just the South Central (SC) United States (Oklahoma and Texas here) anomalies. This was done to reduce computational load required by working with the entire MAMNA dataset.

All the individual girds are first displayed as a total magnetic intensity (TMI) map, which represents the resulting magnetic responses after the main magnetic field of Earth has been removed via IGRF removal. The individual grids were then Reduced-to-Pole (RTP) in order to center anomalies over their causative bodies and correlate them with geologic information

(Baranov, 1957; Baranov and Naudy, 1964; Arkani-Hamed, 1988). RTP filtering values of declination and inclination were taken on the following dates (these represent the rough midpoints for all surveys, or in the case of the MAMNA/NURE data, the rough midpoint of all survey blocks):

Dates are in decimal years.

MAMNA/NURE: 1976.421

2017: 2017.721

Wichita: 1954.833

The Wichita data was then masked to keep effects of knitting with the newer, higher quality, 2017 data to a minimum. In other words, Wichita data was reduced in overall area to the bare minimum, such that it would fill gaps in the 2017 data, but overlap was kept to a minimum, and the coverage by only the 2017 data was maximized. This was done primarily because the Wichita data has sparse to no original survey documentation, as noted by Sweeney and Hill (2005). The result of this is that only a final magnetic anomaly value labeled 'mag_anom' is provided. Similar to what has been noted in NURE data lacking documentation (see Hill et al., 2009), we assume that this represents some processed magnetic value with an undetermined International Geomagnetic Reference Field (IGRF) having been removed. Because a lack of documentation means that the processing cannot be undone, this resulted in large nanotesla (nT) values discrepancies between the 2017 and Wichita data when measured at any overlapping point, even though grids displayed similar structure (i.e. structure was similar in both grids at any given point of overlap). Regardless we opted to mask as much of the Wichita data when possible to limit its influence on final maps.

Grid merging or 'knitting' two grids directly together is a standard process in Oasis Montaj. However, given the limited information regarding the Wichita dataset we modified this knitting method by first leveling the Wichita and 2017 data relative to the MAMNA/NURE data before knitting. The result is a knitted grid that has had its independent sub-grids leveled about a constant value, or the regional MAMNA grid in this case (Oasis Montaj support, personnel communication). After some visual comparisons with grids produced by directly knitting the two grids together this method was deemed to be the best at maintaining structures unique to each dataset, while also providing the most seamless knitting of the grids (i.e. less knitting artifacts) over regions where the individual-grids overlapped. This combined grid was then knitted to the MAMNA data. Individual parameters in the knitting process were left on default settings, as various knitting renditions where these parameters were changed proved to produce limited to no improvements for the grids.

9.0 OTHER DATASETS

9.1 Depth to Basement Data

Well logs used are partially owned by Chesapeake Energy Corporation but were supplemented by Oklahoma Geological Survey (OGS) logs.

The map was hand contoured in GeoGraphix using well data and surface exposure. The top of basement was picked on well logs where available. The top of basement was estimated to be deeper than the total depth of any single well when the well did not penetrate basement. Aeromagnetic, 2D seismic, and tops from wells logs were used to constrain fault geometries. En echelon faults in the south-west part of the map were modified from Heran et al. (2003).

OGS data may be found here:

http://www.ou.edu/ogs/data/oil-gas -- Under "Wells Drilled to Basement" – Table 1 XLS

A summary of the process that went into this OGS compilation may be found here:

http://ogs.ou.edu/docs/specialpublications/SP2006-1.pdf

9.2 Seismic Data

Seismic data is controlled by Chesapeake Energy and by Seismic Exchange Inc (SEI). Uninterpreted sections may be found in Fig. S4.

9.3 Remote Sensing Data

Data was collected at eye altitude of 60 km in the Google Earth program. This eye altitude was chosen in order to remove the effects of smaller scale fractures and bias results towards more regional trends. Ultimately this elevation was chosen after trial and error attempts at high and lower altitudes, which resulted in either too few data or data contaminated by exfoliation fractures, respectively.

CHAPTER III

FUTURE WORK

FUTURE WORK

Avenues for future work in the Southern Oklahoma Aulacogen (SOA) and surrounding region are varied and this section seeks to provide some of the potential areas forfuture work.

1.0 MAGNETOTELLURIC (MT) INVESTIGATIONS

The subsurface structure of the SOA is relatively well defined in the upper 10-15 km due to seismic experiments (e.g. Brewer et al., 1983; Chang et al., 1989) and gravity modelling (Keller and Stephenson, 2007). On the contrary little is known beneath these depths, but these regions provide insight on crustal architecture and paleo-tectonics in the south central United States. As a result we set out to image these regions using Magnetotellurics (MT), a lithosphere imaging electromagnetic method (see Simpson and Bahr, 2005 for a comprehensive understanding of MT). Other paleo-tectonics features have benefited from the use of MT. These studies have uncovered conductive anomalies interpreted as crustal graphite/sulfides, olivine diminution, remnant lithosphere mantle hydration, and mantle metasomatism; which have been help to inform on questions related to the tectonic assembly of North America, crustal architecture, and so forth (Jones et al., 2001; Bedrosian, 2016; Wunderman et al., 2018; DeLucia et al., 2019).

The SOA presents an interesting opportunity for applying MT as a causative mechanism for its localization remains elusive. Further the SOA cuts clear along a suggested terrain

boundary between the Mazatzal and Granite-Rhyolite provinces, while also penetrating deeply into the Mazatzal (Whitmeyer and Karlstrom, 2007; Keller and Stephenson, 2007). Popular theories concerning why the SOA localized include an initial unknown lithosphere weakness which facilitated rift localization (Denison, 1982) a perhaps underreported mobile belt in the region called the Red River mobile belt (Hamilton, 1956 and references therein), or an earlier shear zone (Budnik, 1986). The last of these is a favored interpretation for anomalous conductivity in the recently revealed NW trending Missouri Conductivity Belt, which was suggested to have localized due to a whole-lithosphere rooted trans-North America NW trending shear zone (DeLucia et al., 2019). Interestingly the development, and inversion, of the SOA has been suggested to have occurred on a similar NW trending shear zone (Budnik, 1986), one of many suggested in the North American continent (Paulsen and Marshak, 1994; Thomas, 2011). If a similar shear zone or tectonic weakness is present beneath the SOA it may help to explain the localization of initial rifting, and perhaps the seismicity in the region (as was noted by DeLucia et al., 2019 in the Missouri Belt).

As part of this study, we acquired 13 long period LEMI-417 MT soundings over the SOA. These devices are ideal for imaging the whole lithosphere down to multiple hundreds of kilometers. We spaced 10 of the stations at ~20km over the gravity, magnetic, and historic trace of the SOA, and had 3 additional stations spaced at ~ 50 km off the trace of the SOA. The profile was oriented perpendicular to the strike of the SOA (Fig. 1, below), which is standard practice for collection of MT and adata. The final results of this portion of study are forthcoming, but initial models show the lithosphere beneath the SOA markedly conductive compared to the regions around it. Future work will focus on defining the source of this conductive signature.

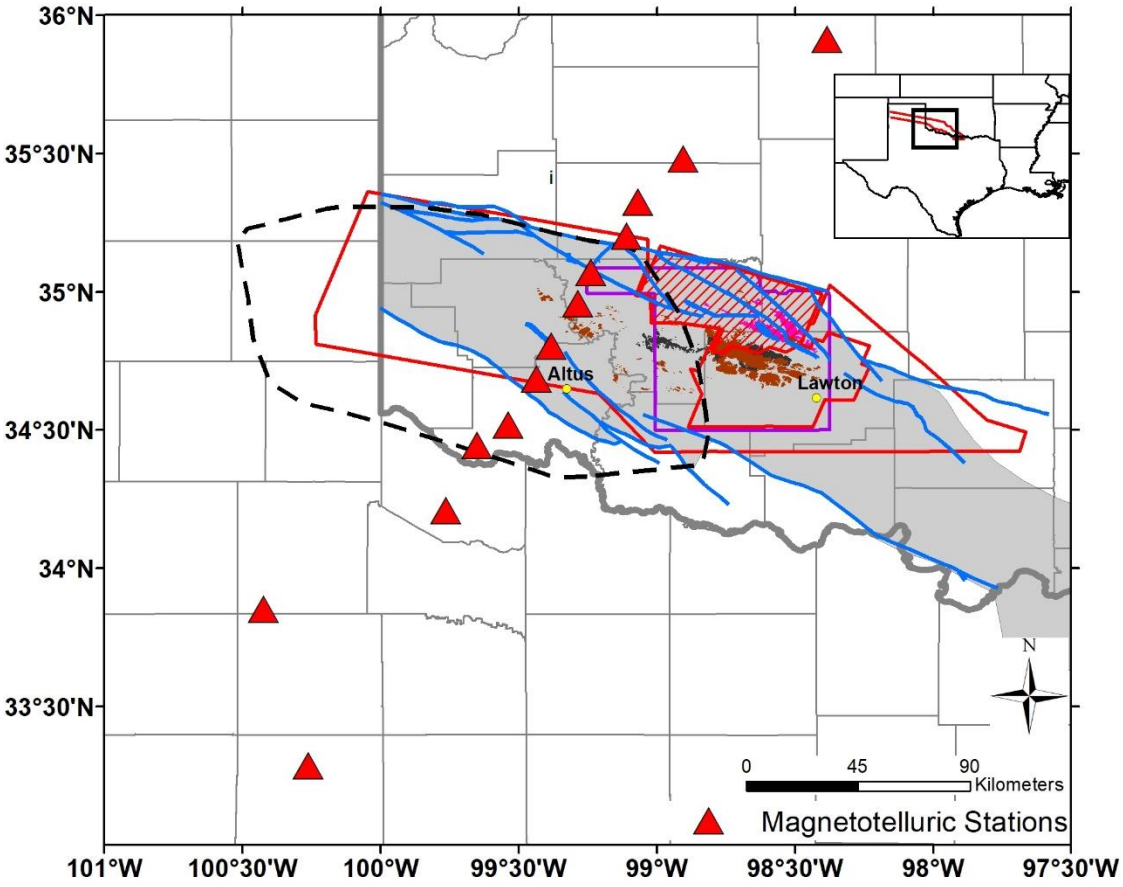

Figure 1. Image showing the locations of the 13 Magnetotelluric stations deployed over the southern Oklahoma Aulacogen in a NE trending profile. Red triangles denote stations.

2.0 SEISMIC HAZARDS

The work in Chapter 2 shows the SOA to be a hazardous ancient tectonic features with NW and E-W trending fault sets. The NW set was shown to be the most active in the modern day, and the most probable hazard for the future; while the E-W set acts as an additional possible hazard. The largest possible fault-related hazards, and thus the areas that deserve the most attention for these sets are the Meers (NW trending) and Willow (E-W trending) faults. While the Meers is a known seismic hazard, we have used the aeromagnetic data to extend its length to ~80 km, and modify its trace with additional splays and other structures not previously recognized. The new Meers trace and associated structures cross additional Quaternary deposits that would allow further paleoseimic studies, which have even recently uncovered previously

unknown paleo-earthquakes along the Meers (Hornsby, 2017). The Willow fault also crosses Quaternary deposits along its length, suggesting paleoseismic studies could be performed along it as well. The traces of both faults are also only shallowly buried in the region (Figs. 2 in Chapter II) meaning accessing them to determine the fault properties which allow for slip along intraplate faults may be possible. Further, while Quaternary ruptures are not present, or at least obvious, for the extended Meers or the Willow this may reflect inherent limits in using obvious quaternary faulting to determine intraplate hazards. This is because long recurrence intervals can lead to burial of hazardous faults, and/or faults may not always break into overlying Quaternary units (Peterson et al. 2014). One possible avenue of use for determining modern scarps along the extended Meers and Willow faults is the collection of LIDAR data. LIDAR has had considerable success delineating hazardous faults when both satellite imagery and digital elevation data have failed (e.g. Lienkaemper et al., 2015).

3.0 THE SOUTHERN OKLAHOMA AULACOGEN AND ANCESTRAL ROCKY MOUNTAIN TECTONICS

As one of the series of Ancestral Rocky Mountain (ARM) uplifts (Fig. 1 in Chapter I) the SOA preserves the kinematics of the poorly understood tectonic processes driving ARM inversion. ARM uplift has a variety of models invoked to explain it (e.g. Leary et al., 2017; Marshak et al., 2000; Ye et al., 1996; Kluth, 1986; Kluth et al., 1998; Kluth and Coney, 1981, among a variety of others) which frequently compete, conflict, compliment and so forth. It is the view of the author that the SOA is perhaps best suited for understanding ARM uplift. This is because unlike the ARM uplifts in Colorado-New Mexico the SOA has escaped reactivation and overprinting by younger tectonic processes like the Rio Grande Rift, Laramide Orogeny and Basin and Range. Further, while the other ARM uplifts in Texas and Oklahoma may have

escaped younger tectonic reactivation many are deeply buried, and thus not readily accessible. This is in contrast to the SOA where one can find both surface exposures of critical structure and/or comparatively limited burial.

A brief analysis of the data presented here suggests that the inversion of the SOA was accommodated via thrust faulting (Brewer et al., 1983; Fig. 3 in Chapter 2) and sinistral strike slip faulting (Fig. 2, 3 in Chapter 2; Granath, 1989), which resulted in NE-SW shortening, and E-W sinistral strike slip movement. The timings of thrust fault movement began in the Pennsylvanian and ended by the Atokon (Brewer et al., 1983), whereas sinistral strike slip movement began in the Pennsylvanian (Granath, 1989) and extends well into the Permian (Fig. 3C in Chapter 2). Within the greater models invoked to explain ARM uplift these trends and timings agree well with the Sonora (Mexico) transpressional model of Leary et al. (2017), which was colliding along the SW section of Laurentian during this time (Domerier and Torsvik, 2014). Given that ARM uplifts represent contemporaneous structural inversion (Schumaker, 1992; Leary et al., 2017) one would expect to see similar fault movements and timings in the other ARM uplifts, and this remains an avenue of research. Additionally, a more comprehensive analysis of SOA structure, as it relates to ARM inversion, is also warranted.

REFERENCES

Al-Shaieb, Z., 1988. Uranium mineralization in the peralkaline Quanah Granite and related pegmatite-aplite dikes, wichita mountains, oklahoma. Ore Geology Reviews, 3(1-3), pp.161-175.

Alt, R.C., & Zoback, M. D., 2017, In Situ Stress and Active Faulting in Oklahoma. Bulletin of the Seismological Society of America, v. 107, p. 1–13, https://doi.org/10.1785/0120160156.

Amsden, T.W., 1982. Early and Middle Paleozoic history of the Anadarko Basin. Geol. Sot. Am., Abstr. Progr., 14(3): 105.

Arkani-Hamed, J., 1988, Differential reduction-to-the-pole of regional magnetic anomalies. Geophysics, 53, p 1592-1600, https://doi.org/10.1190/1.1442441.

Baldridge, W.S., Keller, G.R., Haak, V., Wendlandt, E. and Jiracek, G.R., 1995. The Rio Grande rift in Olsen, KH ed. Continental rifts: evolution, structure, and tectonics: Developments in geotectonics, v. 25.

Bankey, V., et al., 2002, Digital data grids for the magnetic anomaly map of North America: U.S. Geological Survey Open-File Report 02-414, https://doi.org/10.3133/ofr02414.

Baranov, V. and Naudy, H., 1964, Numerical calculation of the formula of reduction to the magnetic pole. Geophysics, 29, p. 67-79, http://dx.doi.org/10.1190/1.1439334.

Baranov, V., 1957, A new method for interpretation of aeromagnetic maps: pseudo-gravimetric anomalies. Geophysics, v. 22, p. 359-382, https://doi.org/10.1190/1.1438369.

Bedrosian, P.A., 2016. Making it and breaking it in the Midwest: Continental assembly and rifting from modeling of EarthScope magnetotelluric data. Precambrian Research, 278, pp.337-361.

Blakely, R. J., Wells, R. E., et al., 2000, New aeromagnetic data reveal large strike-slip (?) faults in the northern Willamette Valley, Oregon }. GSA Bulletin, v. 112, p. 1225–1233.

Boyd, O., Haller, K., Luco, N., Moschetti, M., Mueller, C., Petersen, M., Rezaeian, S. and Rubinstein, J., 2015. Seismic hazard in the nation's Breadbasket. Earthquake Spectra, 31(S1), pp.S109-S130.

Brewer, J. A., Oliver, J. E., Brown, L. D., & Kaufman, S., 1983. COCORP profiling across the Southern Oklahoma aulacogen: Overthrusting of the Wichita Mountains and compression within the Anadarko Basin. Geology, 11, 109–114.

Brewer, J.A., Brown, L.D., Steiner, D., Oliver, J.E., Kaufman, S. and Denison, R.E., 1981. Proterozoic basin in the southern Midcontinent of the United States revealed by COCORP deep seismic reflection profiling. Geology, 9(12), pp.569-575.

Brueseke, M.E., Hobbs, J.M., Bulen, C.L., Mertzman, S.A., Puckett, R.E., Walker, J.D. and Feldman, J., 2016. Cambrian intermediate-mafic magmatism along the Laurentian margin: Evidence for flood basalt volcanism from well cuttings in the Southern Oklahoma Aulacogen (USA). Lithos, 260, pp.164-177.

Budnik, R.T., 1986. Left-lateral intraplate deformation along the Ancestral Rocky Mountains: implications for late Paleozoic plate motions. Tectonophysics, 132(1-3), pp.195-214.

Burke, K. and Dewey, J.F., 1973. Plume-generated triple junctions: key indicators in applying plate tectonics to old rocks. The Journal of Geology, 81(4), pp.406-433.

Crone, A. J., Survey, U. S. G., Luza, K. V, & Geological, O., 1990, Style and timing of Holocene surface faulting on the Meers fault , southwestern Oklahoma. GSA Bulletin, v. 102, p. 1–17.

Cullen, A., 2016. Seismic risk of the Meers Fault, SW Oklahoma: A hoary giant or great imposter. American Association of Petroleum Geologists Search and Discovery Article, (51239), p.21.

Denison, R.E., 1995. Significance of air-photograph linears in the basement rocks of the Arbuckle Mountains, in: Johnson, K.D. (Ed.), Structural Styles in the Southern Midcontinent, 1992 Symposium. Oklahoma Geological Survey Circular 97, pp. 119–131

DeLucia, M.S., Murphy, B.S., Marshak, S. and Egbert, G.D., 2019. The Missouri High-Conductivity Belt, revealed by magnetotelluric imaging: Evidence of a trans-lithospheric shear zone beneath the Ozark Plateau, Midcontinent USA?. Tectonophysics, 753, pp.111-123.

Dickerson, P.W., 2003. Intraplate mountain building in response to continent–continent collision—the Ancestral Rocky Mountains (North America) and inferences drawn from the Tien Shan (Central Asia). Tectonophysics, 365(1-4), pp.129-142.

Domeier, M. and Torsvik, T.H., 2014. Plate tectonics in the late Paleozoic. Geoscience Frontiers, 5(3), pp.303-350.

Donovan, R.N., 1982. Geology of Blue Creek Canyon, Wichita Mountains area. Geology of the eastern Wichita Mountains, southwestern Oklahoma: Oklahoma Geological Survey Guidebook, 21, pp.65-77.

Ewing, T.E., Budnik, R.T., Ames, J.T., Ridner, D.M. and Dillon, R.L., 1990, Tectonic map of Texas: The University of Texas at Austin. Bureau of Economic Geology, scale, 1:750,000, p.4.

Gilbert, M.C., 1983. Timing and chemistry of igneous events associated with the southern Oklahoma aulacogen. In Developments in Geotectonics (Vol. 19, pp. 439-455). Elsevier.

Gordon, D. W., 1988, Revised instrumental hypocenters and correlation of earthquake locations and tectonics in the central United States, U.S. Geological Survey Professional Paper 1364, 69 p.

Granath, J.W., 1989. Structural evolution of the Ardmore Basin, Oklahoma: Progressive deformation in the foreland of the Ouachita collision. Tectonics, 8(5), pp.1015-1036.

Grauch VJS, Hudson MR. 2007. Guides to understanding the aeromagnetic expression of faults in sedimentary basins: lessons learned from the central Rio Grande Rift, New Mexico. Geosphere 3(6): 596–623. DOI: 10.1130/GES00128.1

Grauch, V.J.S. and Hudson, M.R., 2011. Aeromagnetic anomalies over faulted strata. The Leading Edge, 30(11), pp.1242-1252.

Ham, W.E., 1964. Basement Rocks and Structual Evolution of Southern Oklahoma. The Mountain Geologist.

Hamilton, W.B., 1956. Precambrian rocks of Wichita and Arbuckle Mountains, Oklahoma. Geological Society of America Bulletin, 67(10), pp.1319-1330.

Hanson, R.E., Puckett Jr, R.E., Keller, G.R., Brueseke, M.E., Bulen, C.L., Mertzman, S.A., Finegan, S.A. and McCleery, D.A., 2013. Intraplate magmatism related to opening of the southern Iapetus Ocean: Cambrian Wichita igneous province in the Southern Oklahoma rift zone. Lithos, 174, pp.57-70.

Heidbach, O. et al., 2018, The World Stress Map database release 2016: Crustal stress pattern across scales. Tectonophysics, v. 744, p. 484-498, https://doi.org/10.1016/j.tecto.2018.07.007.

Heran, W.D., Green, G.N. and Stoeser, D.B., 2003. A digital geologic map database for the state of Oklahoma (No. 2003-247).

Hill, P.L., Kucks, R.P. and Ravat, D., 2009. Aeromagnetic and aeroradiometric data for the conterminous United States and Alaska from the National Uranium Resource Evaluation (NURE) Program of the US Department of Energy (No. 2009-1129). US Geological Survey.

Hills, J. M. (1970). Late Paleozoic Structural Directions in Southern Permian Basin , West Texas and Southeastern New Mexico AAPG Bulletin, 10(10), 1809–1827.

Hoffman, P., Dewey, J.F. and Burke, K., 1974. Aulacogens and their genetic relation to geosynclines with a Proterozoic example from Great Slave Lake Canada.

Hogan, J.P. and Gilbert, M.C., 1998. The Southern Oklahoma aulacogen: A Cambrian analog for Mid-Proterozoic AMCG (anorthosite-mangerite-charnockite-granite) complexes?. In Basement tectonics 12 (pp. 39-78). Springer, Dordrecht.

Hornsby, K.T., 2017, Constraining the Holocene Extent of the Northwest Meers Fault, Oklahoma Using High-Resolution Topography and Paleoseismic Trenching [MS Thesis]: Portland, Portland State University, 124 p, http://doi.org/10.15760/etd.5778.

Hough, S.E., Armbruster, J.G., Seeber, L. and Hough, J.F., 2000, On the modified Mercalli intensities and magnitudes of the 1811–1812 New Madrid earthquakes. Journal of Geophysical Research: Solid Earth, v. 105, p. 23839-23864, https://doi.org/10.1029/2000JB900110.

Jacobsen, B.H., 1987, A case for upward continuation as a standard separation filter for potential-field maps. Geophysics, v. 52, p. 1138-1148, https://doi.org/10.1190/1.1442378.

Johnson, E.L., 1955. Geology of the pegmatites in the Hale Spring area, Wichita Mountains, Oklahoma. M.S. Thesis, Univ. of Oklahoma, Norman, Okla., 87 pp.

Jones, A.G., Ferguson, I.J., Chave, A.D., Evans, R.L. and McNeice, G.W., 2001. Electric lithosphere of the Slave craton. Geology, 29(5), pp.423-426.

Jones-Cecil, M., 1995, Structural controls of Holocene reactivation of the Meers fault, southwestern Oklahoma, from magnetic studies. Geological Society of America Bulletin, v. 107, p. 98-112.

Katz, O., Gilbert, M.C., Reches, Z. and Roegiers, J.C., 2001, Mechanical properties of Mount Scott granite, Wichita Mountains, Oklahoma. Oklahoma Geology Notes, v. 61, p. 28-34.

Keller, G.R., Stephenson, R.A., 2007, The southern Oklahoma and Dniepr-Donets aulacogens: A comparative analysis. Memoirs-Geological Society of America, v. 200, p. 127, https://doi.org/10.1130/2007.1200(08).

King, P.B. and Henbest, L.G., 1965. Geology of the Sierra Diablo region, Texas. US Government Printing Office.

Kluth, C.F. and Coney, P.J., 1981. Plate tectonics of the ancestral Rocky Mountains. Geology, 9(1), pp.10-15.

Kluth, C.F., 1986. Plate tectonics of the ancestral rocky mountains: part III. Middle rocky mountains.

Kluth, C.F., Ye, H., Royden, L., Burchfiel, C. and Schuepbach, M., 1998. Late Paleozoic Deformation of Interior North America: The Greater Ancestral Rocky Mountains: Discussion & Reply. AAPG bulletin, 82(12), pp.2272-2276.

Kolawole, F., Atekwana, E.A., Laó-Dávila, D.A., Abdelsalam, M.G., Chindandali, P.R., Salima, J. and Kalindekafe, L., 2018. High-resolution electrical resistivity and aeromagnetic imaging reveal the causative fault of the 2009 M w 6.0 Karonga, Malawi earthquake. Geophysical Journal International, 213(2), pp.1412-1425.

Kolawole, F., Atekwana, E.A., Laó-Dávila, D.A., Abdelsalam, M.G., Chindandali, P.R., Salima, J. and Kalindekafe, L., 2018, High-resolution electrical resistivity and aeromagnetic imaging reveal the causative fault of the 2009 M w 6.0 Karonga, Malawi earthquake. Geophysical Journal International, v. 213, p. 1412-1425, https://doi.org/10.1002/2017TC004628.

Kolawole, F., Atekwana, E.A., Malloy, S., Stamps, D.S., Grandin, R., Abdelsalam, M.G., Leseane, K. and Shemang, E.M., 2017. Aeromagnetic, gravity, and Differential Interferometric Synthetic Aperture Radar analyses reveal the causative fault of the 3 April 2017 Mw 6.5 Moiyabana, Botswana, earthquake. Geophysical Research Letters, 44(17), pp.8837-8846.

Kolawole, F., Johnston, C., Chang, J., Marfurt, K. J., Reches, Z., & Carpenter, B. M., 2018b. Characterization of pre-existing structures in the basement of Oklahoma with implications for induced seismicity. GSA Annual Meeting in Indianapolis, Indiana Paper No. 158-6.

Lambert, D.D., Unruh, D.M., Gilbert, M.C., 1988. Rb–Sr and Sm–Nd isotopic study of the Glen Mountains Layered Complex: Initiation of rifting within the Southern Oklahoma aulacogen. Geology 16, 13–17.

Leary, R. J., Umhoefer, P., Smith, M. E., & Riggs, N. (2018). A three-sided orogen: A new tectonic model for Ancestral Rocky Mountain uplift and basin development. Geology, 45(8), 735–738. https://doi.org/10.1130/G39041.1

Levandowski, W., Zellman, M., & Briggs, R. (2017). Gravitational body forces focus North American intraplate earthquakes. Nature Communications, 8, 1–9. https://doi.org/10.1038/ncomms14314

Lienkaemper, J.J., DeLong, S.B., McPherson, R.C., Mielke, J., Avdievitch, N., Pickering, A. and Lloyd, C., 2014, December. Characterizing Recent Slip on the Kuikui Fault, a Link Between the Green Valley and Bartlett Springs Fault Zones, Wilson Valley, Northern California. In AGU Fall Meeting Abstracts.

Liu, M. and Stein, S., 2016, Mid-continental earthquakes: Spatiotemporal occurrences, causes, and hazards. Earth-Science Reviews, v. 162, p. 364-386, http://dx.doi.org/10.1016/j.earscirev.2016.09.016.

Snee, J.E.L. and Zoback, M.D., 2016, State of stress in Texas: Implications for induced seismicity. Geophysical Research Letters, v. 43, p. 10-208, https://doi.org/10.1002/2016GL070974.

Magnani, M.B., Blanpied, M.L., DeShon, H.R. and Hornbach, M.J., 2017, Discriminating between natural versus induced seismicity from long-term deformation history of intraplate faults. Science advances, v. 3(11), p. e1701593, https://doi.org/10.1126/sciadv.1701593

Marsh, S. and Holland, A., 2016, Comprehensive fault database and interpretive fault map of Oklahoma. Oklahoma Geological Survey Open-File Rept., p. 15.

Marshak, S., Karlstrom, K. and Timmons, J.M., 2000. Inversion of Proterozoic extensional faults: An explanation for the pattern of Laramide and Ancestral Rockies intracratonic deformation, United States. Geology, 28(8), pp.735-738.

Marshak, S., Nelson, W.J. and McBride, J.H., 2003. Phanerozoic strike-slip faulting in the continental interior platform of the United States: examples from the Laramide Orogen, Midcontinent, and Ancestral Rocky Mountains. Geological Society, London, Special Publications, 210(1), pp.159-184.

McConnell, D.A. and Gilbert, M.C., 1990. Cambrian extensional tectonics and magmatism within the Southern Oklahoma Aulacogen. Tectonophysics, 174(1-2), pp.147-157.

McConnell, D.A., 1989. Determination of offset across the northern margin of the Wichita uplift, southwest Oklahoma. Geological Society of America Bulletin, 101(10), pp.1317-1332.

McLean, T.R. and Stearns, D.W., 1986, Stop 7: Hale spring locality. Petrology of the Cambrian Wichita Mountains Igneous Suite in Oklahoma Geological Survey, Guidebook, v. 23, p. 172-178.

McNamara, D.E., Benz, H.M., Herrmann, R.B., Bergman, E.A., Earle, P., Meltzer, A., Withers, M. and Chapman, M., 2013, The Mw 5.8 Mineral, Virginia, earthquake of August 2011 and aftershock sequence: Constraints on earthquake source parameters and fault geometry. Bulletin of the Seismological Society of America, v. 104, p. 40-54, https://doi.org/10.1785/0120130058.

Miller, H.G. and Singh, V., 1994. Potential field tilt—a new concept for location of potential field sources. Journal of Applied Geophysics, 32(2-3), pp.213-217.

Myers, J.D., Gilbert, M.C. and Loiselle, M.C., 1981. Geochemistry of the Cambrian Wichita Granite Group and revisions of its lithostratigraphy. Oklahoma Geology Notes, 41(6), pp.172-195.

Nelson, J.D., Chao, K.C., Overton, D.D. and Nelson, E.J., 2015. Foundation engineering for expansive soils (p. 416). New York: Wiley.

Paulsen, T. and Marshak, S., 1994. Cratonic weak zone in the US continental interior: The Dakota-Carolina corridor. Geology, 22(1), pp.15-18.

Perry, W.J., 1989, Tectonic evolution of the Anadarko Basin region, Oklahoma: U.S. Geological Survey Bulletin 1866-A, 19 p, https://doi.org/10.3133/b1866A.

Petersen, M.D. et al., 2014, Documentation for the 2014 update of the United States national seismic hazard maps: U.S. Geological Survey Open-File Report 2014–1091, 243 p., https://dx.doi.org/10.3133/ofr20141091.

Powell, B.N., Gilbert, M.C. and Fischer, J.F., 1980. Lithostratigraphic classification of basement rocks of the Wichita province, Oklahoma: Summary. Geological Society of America Bulletin, 91(9), pp.509-514.

Pratt, T.L., Hauser, E.C. and Nelson, K.D., 1992. Widespread buried Precambrian layered sequences in the US mid-continent: Evidence for large proterozoic depositional basins (1). AAPG Bulletin, 76(9), pp.1384-1401.

Shah, A.K., and Finn, C.A., 2018, Airborne Magnetic Surveys over Oklahoma, 2017: U.S. Geological Survey data release, https://doi.org/10.5066/F7ZG6RJP.

Shumaker, R.C., 1992. Paleozoic Structure of the Central Basin Uplift and Adjacent Delaware Basin, West Texas (1). AAPG Bulletin, 76(11), pp.1804-1824.

Simpson, F. and Bahr, K., 2005. Practical magnetotellurics. Cambridge University Press.

Skulski, T., Francis, D. and Ludden, J., 1991. Arc-transform magmatism in the Wrangell volcanic belt. Geology, 19(1), pp.11-14.

Skulski, T., Francis, D. and Ludden, J., 1992. Volcanism in an arc-transform transition zone: the stratigraphy of the St. Clare Creek volcanic field, Wrangell volcanic belt, Yukon, Canada. Canadian Journal of Earth Sciences, 29(3), pp.446-461.

Snee, J.E.L. and Zoback, M.D., 2016, State of stress in Texas: Implications for induced seismicity. Geophysical Research Letters, v. 43, p. 10-208, https://doi.org/10.1002/2016GL070974.

Stein, C.A., Stein, S., Merino, M., Randy Keller, G., Flesch, L.M. and Jurdy, D.M., 2014. Was the Midcontinent Rift part of a successful seafloor-spreading episode?. Geophysical Research Letters, 41(5), pp.1465-1470.

Sweeney, R.E. and Hill, P.L., 2005. Nebraska, Kansas, and Oklahoma aeromagnetic and gravity maps and data: a web site for distribution of data (No. 138).

Thomas, W.A., 1991. The Appalachian-Ouachita rifted margin of southeastern North America. Geological Society of America Bulletin, 103(3), pp.415-431.

Thomas, W.A., 2011. The Iapetan rifted margin of southern Laurentia. Geosphere, 7(1), pp.97-120.

Tuttle, M.P., Schweig, E.S., Sims, J.D., Lafferty, R.H., Wolf, L.W. and Haynes, M.L., 2002. The earthquake potential of the New Madrid seismic zone. Bulletin of the Seismological Society of America, 92(6), pp.2080-2089.

CEUS-SSCN, 2012, Central and Eastern United States seismic source characterization for nuclear facilities: Palo Alto, California, EPRI, U.S. DOE, and U.S. NRC, [variously paged]. (Aviliable for download at http://www.ceus-ssc.com/Report/Downloads.html.)

Verduzco, B., Fairhead, J.D., Green, C.M. and MacKenzie, C., 2004. New insights into magnetic derivatives for structural mapping. The Leading Edge, 23(2), pp.116-119.

Wall, C.J., Hanson, R., Schmitz, M., Price J.D., Donovan, N., 2019. Age of the wichita igneous province: integrating zircon geochronological and geochemical constraints on voluminous Cambrian magmatism in the southern Oklahoma aulacogen

Wall, C.J., Schmitz, M., Hanson, R., Price J.D., Donovan, N., 2018. Precise U-PB geochronological constrains on voluminous cambrian magmatism in the southern oklahoma aulacogen. Geologic Society of America Annual Meeting – Indianapolis, IN. doi: 10.1130/abs/2018AM-323162

Walsh III, F.R. and Zoback, M.D., 2016, Probabilistic assessment of potential fault slip related to injection-induced earthquakes: Application to north-central Oklahoma, USA. Geology, v. 44, p.9 91-994, https://doi.org/10.1130/G38275.1.

Walter, J.I., Frohlich, C. and Borgfeldt, T., 2018, Natural and Induced Seismicity in the Texas and Oklahoma Panhandles. Seismological Research Letters, v. 89, p. 2437-2446, https://doi.org/10.1785/0220180105.

Whitmeyer, S.J. and Karlstrom, K.E., 2007. Tectonic model for the Proterozoic growth of North America. Geosphere, 3(4), pp.220-259.

Wunderman, R.L., Wannamaker, P.E. and Young, C.T., 2018. Architecture of the hidden Penokean terrane suture and Midcontinent rift system overprint in eastern Minnesota and western Wisconsin from magnetotelluric profiling. Lithosphere, 10(2), pp.291-300.

Ye, H., Royden, L., Burchfiel, C., & Schuepbach, M. (1996). Late Paleozoic Deformation of Interior North America : The Greater Ancestral Rocky Mountains 1. AAPG Bulletin, 9(9), 1397–1432.

VITA

Brandon Franklin Werner Chase

Candidate for the Degree of

Master of Science

Thesis: HIGH RESOLUTION GEOPHYSICAL IMAGING REVEALS MAJOR FAULTS IN THE SOUTHERN OKLAHOMA AULACOGEN: IMPLICATIONS FOR MID-CONTINENT SEISMIC HAZARDS

Major Field: Geology

Biographical:

Education:

Completed the requirements for Masters of Science in Geology at Oklahoma State University, Stillwater, Oklahoma in May, 2019

Completed the requrements for Bachelors of Arts in Geology at the University of Colorado, Boulder, Colorado in 2016

Experience:

Graduate teaching assistant for Physical Geology

Graduate teaching assistant for Geology and Human Affiars

Head teaching assistant for Physical Geology

Contractors for United States Geologic Survey Crustal Geophysics and Geochemistry Science Center

Professional Memberships

SEG, AGU, and GSA, all student memberships.